REVIEW

Melt Electrospinning

ADVANCED
FUNCTIONAL
MATERIALS

www.afm-journal.de

The Next Frontier in Melt Electrospinning: Taming the Jet

Thomas M. Robinson, Dietmar W. Hutmacher,* and Paul D. Dalton*

There is a specialized niche for the electrohydrodynamic jetting of melts, from biomedical products to filtration and soft matter applications. The next frontier includes optics, microfluidics, flexible electronic devices, and soft network composites in biomaterial science and soft robotics. The recent emphasis on reproducibly direct-writing continual molten jets has enabled a spectrum of contemporary microscale 3D objects to be fabricated. One strong suit of melt processing is the capacity for the jet to solidify rapidly into a fiber, thus fixing a particular structure into position. The ability to direct-write complex and multiscaled architectures and structures has greatly contributed to a large number of recent studies, explicitly, toward fiber–hydrogel composites and fugitive inks, and has expanded into several biomedical applications such as cartilage, skin, periosteum, and cardiovascular tissue engineering. Following the footsteps of a publication that summarized melt electrowriting literature up to 2015, the most recent literature from then until now is reviewed to provide a continuous and comprehensive timeline that demonstrates the latest advances as well as new perspectives for this emerging technology.

1. Introduction

Research into the electrohydrodynamic (EHD) processing of polymer melts has gradually increased over the past decades with a primary driver being the field of biomedical materials and devices.[1] The potential breadth of uses is considerable and mirrors that for solution electrospinning (SES);[2] textiles and membranes with various applications including disposable sanitary and surgical fabrics, filtration, high-performance automotive and aerospace, construction, and soft

T. M. Robinson, Prof. P. D. Dalton
Department of Functional Materials in Medicine
and Dentistry and Bavarian Polymer Institute
University Clinic Würzburg
Pleicherwall 2, Würzburg 97070, Germany
E-mail: paul.dalton@fmz.uni-wuerzburg.de
Prof. D. W. Hutmacher
Institute for Health and Biomedical Innovation
Queensland University of Technology
60 Musk Ave, Kelvin Grove 4059, Australia
E-mail: dietmar.hutmacher@qut.edu.au

The ORCID identification number(s) for the author(s) of this article can be found under https://doi.org/10.1002/adfm.201904664.

robotic materials. Furthermore, there are material-driven challenges that include replacing cotton-based products and "green" manufacturing that eliminates solvent-use during manufacturing.[3] In 2016, Brown et al. published a comprehensive review on melt electrospinning (MES) that encompassed all of the previously known literature in the field.[4] In this review, we summarize the literature since 2015, to provide a continuous and comprehensive summary of how the field of MES is evolving.

2. Historical Perspective

From 2016 onward there has been a significant increase in the number of scientific publications. Over 40 MES and melt electrowriting (MEW) journal articles were published in 2018, and more than 130 MES/MEW journal articles have been published since 2016, as opposed to 89 publications between 2010 and 2015. **Figure 1**A shows the categorization of these publications into either MES or MEW. Of note, the majority of journal articles published within 2018 are for MEW (Figure 1A) demonstrating a shift from the more traditional MES to the modern MEW. Although MES and MEW are both EHD technologies, this recent change in publication focus suggests that the extraordinary control of melt electrospun fiber placement provides benefits for many applications. Many research groups have contributed to the MES/MEW literature since 2016, and several commercial MEW printers are now available (Table 1, Supporting Information). The geographical coauthor distribution since 2015 primarily involved the European Union, Australia, and China, followed by the United States, Canada, and Japan, and have all contributed to the recent literature (Figure 1B).

After the conception of the MEW approach in 2011,[5] it has been described within literature via a range of different terminology, including direct-writing MES;[6] melt EHD 3D printing;[7] and near-field MES.[8] Our terminology has also evolved, with melt electrowriting (derived from "melt electrostatic writing") now distinct to MES, derived from the definition from one of the pioneers in the field "melt electrostatic spinning" by Daryl Reneker in 1995.[9] This terminology is based on the different EHD phenomena that define these two processes.[10] MEW is particularly well suited to accurately direct-write fluid jets without electrical instabilities.

Broadly speaking, there have been several scientific breakthroughs in MEW research over the past four years that significantly contribute to EHD melt processing. These include

1. Controlling "fiber pulsing"; an unstable MEW processing zone that affects both fiber placement and diameter, particularly with increasing build height.[11]
2. Exploiting dynamic electric fields during printing to overcome the charges within the constructs for large volume scaffolds with high and reproducible precision.[12]
3. Digitization of the electrified molten jet to provide both in-process quality control and a reproducible outcome.[13]
4. Processing a wide range of polymers beyond the "gold standard" poly(ε-caprolactone) (PCL).[14]
5. Demonstrating that MEW fiber designs significantly enhances the mechanical properties of soft network composites.[15]

3. Taming the Jet

The major shift of MES/MEW publications since 2015 (Figure 1A) has been due to the better understanding of the Taylor cone and the ability to control the direct writing of the molten jet. The key processing parameters to achieve a highly controlled and reproducible MEW process have been investigated and identified as i) mass flow rate to the nozzle, ii) collector speed and iii) electric field, while the viscosity and charge of the fluid define the properties of the molten polymer. These parameters work in concert to achieve a stable processing region that allows a spectrum of MEW laydown patterns. Establishing the precise balance of each respective parameter has opened further opportunities, such as large voluminous and highly ordered structures. Here, we describe some printing phenomenon, required parameters to identify and MEW designs that result from "taming the jet."

3.1. Fiber Pulsing

It is well known that MES is based on the EHD concept that employs an electric field and a form of heating to draw a continuous polymer melt directly from the spinneret to a collector.[4] Distinct to conventional MES, MEW requires the applied voltage to stabilize the jet while direct writing onto a translating collector (**Figure 2**A).[5] Therefore, when the mass flow to/from the jet is not in equilibrium fiber pulsing predominates leading to material being released at periodic intervals. This unstable flight path causing the unpredictable deposition of fibers and introduces artifacts into the print.[16] Fiber pulsing is due to a combination of parameters—the voltage and mass flow rates being the two greatest known variables to induce/remove fiber pulsing.[11]

3.2. Critical Translation Speed

The direct writing of straight fibers is established when the computer-controlled collector speed is higher than the ultimate jet speed (Figure 2B), termed the critical translation speed (CTS).[11] When operating well above this CTS (Figure 2C), the fiber can be stretched to obtain diameters down to submicrometer size.[17] While processing below this CTS value, however, nonlinear fluid patterns due to jet buckling can be

Thomas M. Robinson is an international double Master's degree student in biofabrication from the University of Wollongong, Australia, and the University of Würzburg, Germany. He holds a B.Sc. degree in medicinal chemistry from the University of Wollongong where he worked within industry at ANSTO. Since 2017, he has worked in several countries and committed to innovation accelerator programs, including helping to bring new technologies to industry. His research interests include the digitalization of melt electrowriting through printomics and advanced soft robotic materials for use within biofabrication.

Dietmar W. Hutmacher is the Director of the Centre in Regenerative Medicine and Director of the ARC Centre in Additive Biomanufacturing at QUT. He holds an M.B.A. degree from the Royal Henley Management College and a Ph.D. degree from NUS. He is a founding member of the International Fellows of TERMIS and was elected into the International College of Fellows Biomaterials Science and Engineering. His has a distinctive educational and scholarly career, combined with industry experience.

Paul D. Dalton is a Professor in Biofabrication at the University of Würzburg, Germany. He is originally from Perth, Australia, where he worked on an artificial cornea through research to the clinic. He became a world traveler, with post-doctoral positions at the University of Toronto, RWTH Aachen, and the University of Southampton. As faculty, he split his time between Shanghai Jiao Tong University, China and QUT, Brisbane, Australia, until 2014. With over 25 years' experience across several disciplines, he pioneered melt electrowriting as a distinct class of additive manufacturing.

observed (Figure 2E–G). These types of patterns are typical of fluid columns impacting on a flat, slowly moving collectors.[18] The rapid solidification of the melt, however, allows such fluid structures to be fixed into place. Shapes such as sinusoidal,
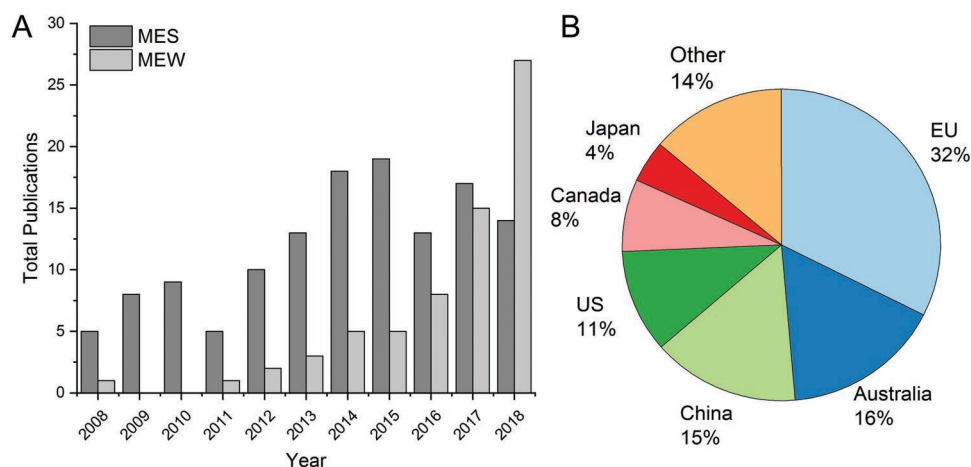
Figure 1. A) Comparison of the total number of journal articles for MES/MEW over the past decade and B) the geographical distribution of coauthors since 2015.

side-loops, "figure of eight," and circular coiling predominate below the CTS[5,11,19] (Figure 2E–G).

3.3. MEW Processing Parameters

Several MEW process parameters have been extensively investigated. Tourlomousis et al. methodically defined the downstream pulling and upstream resistive forces to be balanced in combination with the CTS to achieve a steady equilibrium printing state.[20] Xu et al. similarly examined the electrodynamics and the processability of conventional MES to define the solidification point, jet velocity, fiber diameters and fiber patterns through a temperature-voltage phase diagram.[21] Dayan et al. utilized a response surface methodology model, demonstrating that the collector speed, collector distance and pressure also
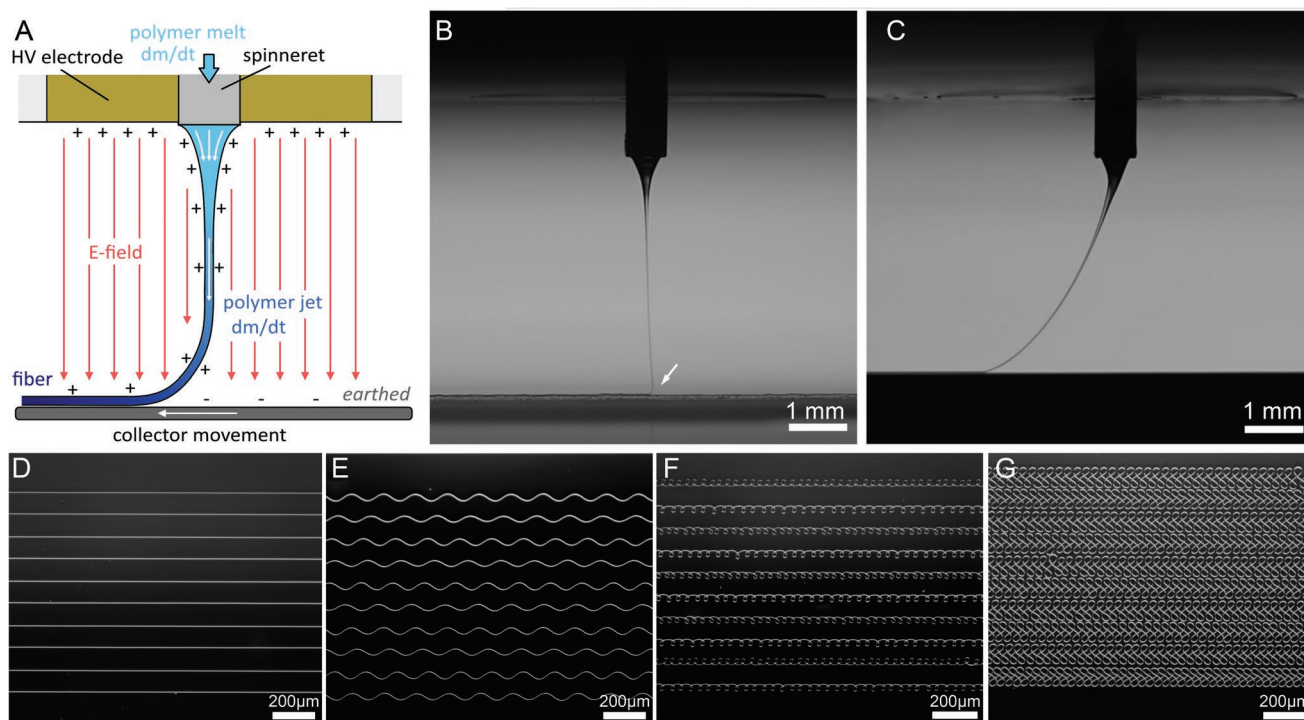
Figure 2. Stable MEW jets. A) A schematic of a molten jet that is direct-written onto a substrate in equilibrium so that the feed rate to the spinneret matches that of the high voltage stabilized polymer jet to avoid fiber pulsing. Images of a PCL MEW jet direct-written B) at the critical translation speed (CTS) on a flat collector with the jet "heel" (white arrow) indicated and C) above the CTS on a cylindrical mandrel. A series of fibers deposited at increasingly lower collector speeds, starting D) above the CTS, E) x0.75 CTS, F) x0.35 CTS, and G) x0.10 CTS. A) Reproduced under the terms and conditions of the Creative Commons CC BY-NC-ND 3.0 License.[11] Copyright 2016, The Authors, published by De Gruyter, B,C) previously unpublished, and D–G) reproduced under the terms and conditions of the Creative Commons CC BY-NC-ND 3.0 License.[11] Copyright 2016, The Authors, published by De Gruyter.

1904664 (3 of 28)

**ADVANCED
SCIENCE NEWS**

www.advancedsciencenews.com

**ADVANCED
FUNCTIONAL
MATERIALS**

www.afm-journal.de

had significant effects on fiber diameter.[22] Ko et al. studied the effect of fiber diameter based on temperature and different molecular weight PCL, describing that fiber diameter would increase with a lower melt viscosity.[23] In addition, it was observed that fiber diameters would decrease with temperature increments revealed by the polymer being able to elongate and be stretched further.[23] This is contradictory to a more recent study,[13] where the lower viscosity due to higher temperatures results in a greater mass flow to the nozzle, resulting in a larger fiber diameter rather than a smaller one. However, this study was performed with air pressure rather than a syringe pump to drive the melt to the nozzle, highlighting how different MEW printer components can result in different processing outcomes.

3.4. Electric Field

Due to the semiconductive nature of many molten polymers, an excess charge from the print head is trapped within each deposited polymer fiber and subsequently counteracts accurate placement of successive fibers with increasing electrical repulsion per layer. Therefore, when printing above the initial induced charge threshold it is important to at least maintain the electrostatic forces at a constant level. This critical parameter has been covered in much detail for the MEW of highly ordered and large volume scaffolds.[12] Brown et al. previously covered the critical aspects of the charge phenomena when performing SES[4] while more recently, this repulsive–attractive phenomenon specifically related to MEW has been further studied to better understand fiber alignment accuracy in regards to residual charge effects.[24] A charge distribution model supported by experimental results was used to define the charge transport pathway during the fiber printing process. The collector material has significant implication with regards to the electric field and charge dissipation.[24] With the notable exception of a publication by Ding et al., the impact of charge on the processing conditions is not well studied within the MEW community.

3.5. MEW Workflow

A standard workflow for the next generation of MEW designs using new polymers will likely involve three major stages: i) parameter screening, ii) dimension-based design, and iii) application. In screening, essential parameters are altered, ideally digitally, to identify their specific effects on final MEW outcomes.[25] Typically, an easily modifiable polymer material (for example, PCL) is selected for high-throughput production (Printomics; as described later) and iterations. The dataset generated, either manually or via jet visualization software,[13] is then assessed for process stability, starting with the control of the mass flow rate to eliminate fiber pulsing. Identifying the CTS, minimum fiber spacing, fiber bridging, and build height accuracy are also essential. This is further used to identify the effects of all system parameters on the proposed scaffold design and guides into the second stage, dimension-based design, where the parameters required for known dimension outcomes are applied in sequence, with fine tuning of the processing

parameters for more complex scaffold architectures. These include accurate fiber spacing (including with build height) and dynamic changes in parameters such as electrical field,[12] or manipulating out-of-plane fiber placement[26] if this is required. The final application stage is more conventional in that a small number of designs that can be assessed for their functionality for specifically designed applications. One can follow these steps when looking to utilize MEW samples for their own research using either house-built or commercial printers. With this parameter control, we see the field of MEW now breaking into the second stage of "taming the jet" to enable more advanced architectures. Digitization through the use of an in-process monitoring system that is capable of defining the process stability of MEW provides a powerful addition to these three major steps for MEW processing.[13]

3.6. MEW Designs

With stable processing established by the elimination of fiber pulsing, there are a multitude of laydown patterns that have already been achieved, including the ability to alter the diameter of the fiber significantly through speed or pressure during a print.[17] Similar to melt extrusion 3D printing in regard to computer-aided design (CAD) software, a layer-by-layer deposition is effectively repeated until the desired complex scaffold is fabricated. Moreover, adjusting the CTS of the collector can further control these patterned designs. Significantly thicker scaffolds can be fabricated as demonstrated by maintaining the height between the print head and the top of the sample as well as simultaneously increasing the applied voltage.[12] Alternatively, multiphasic MEW structures can be fabricated in a single step by controlling the fiber diameter during printing.[17]

The precise deposition and small diameter fibers provide constructs with a high surface to volume ratio.[27] In addition, the ordered placement of small diameter MEW fibers can be used in biomimetic soft network composites.[28] Altering the fiber laydown allows the control the mechanical properties. **Figure 3** shows a number of complex scaffold designs fabricated via MEW ranging from biomedical, lab-on-a-chip to soft robotic applications.

Youssef et al. reported multiple laydown patterns and interfiber spacing to produce scaffolds with different porosities and pore designs,[29] including regular squares, triangular/hexagon (Figure 3A,B), octagon, and dodecagon (Figure 3C,D) designs. Furthermore, the pore morphology and histographical distribution were defined for each fabricated MEW construct by using high-resolution sub-micro computed tomography (μCT). Video S1 (Supporting Information) provides a direct contrast in the porosity distribution between different laydown patterns. Bas et al. developed the first in silico MEW model for soft network composites, including anterior longitudinal ligament (Figure 3E), masseter muscle (Figure 3F) and skin (Figure 3G). Specifically, each of these MEW scaffolds combined the different elements relating to their engineered tissues, such as functioning under high tensile loads.[30] Likewise, Saidy et al. manufactured medical-grade PCL constructs with a sinusoidal microarchitecture that mimics the wavy-like architecture of native collagen fibers. Figure 3H shows such an MEW scaffold
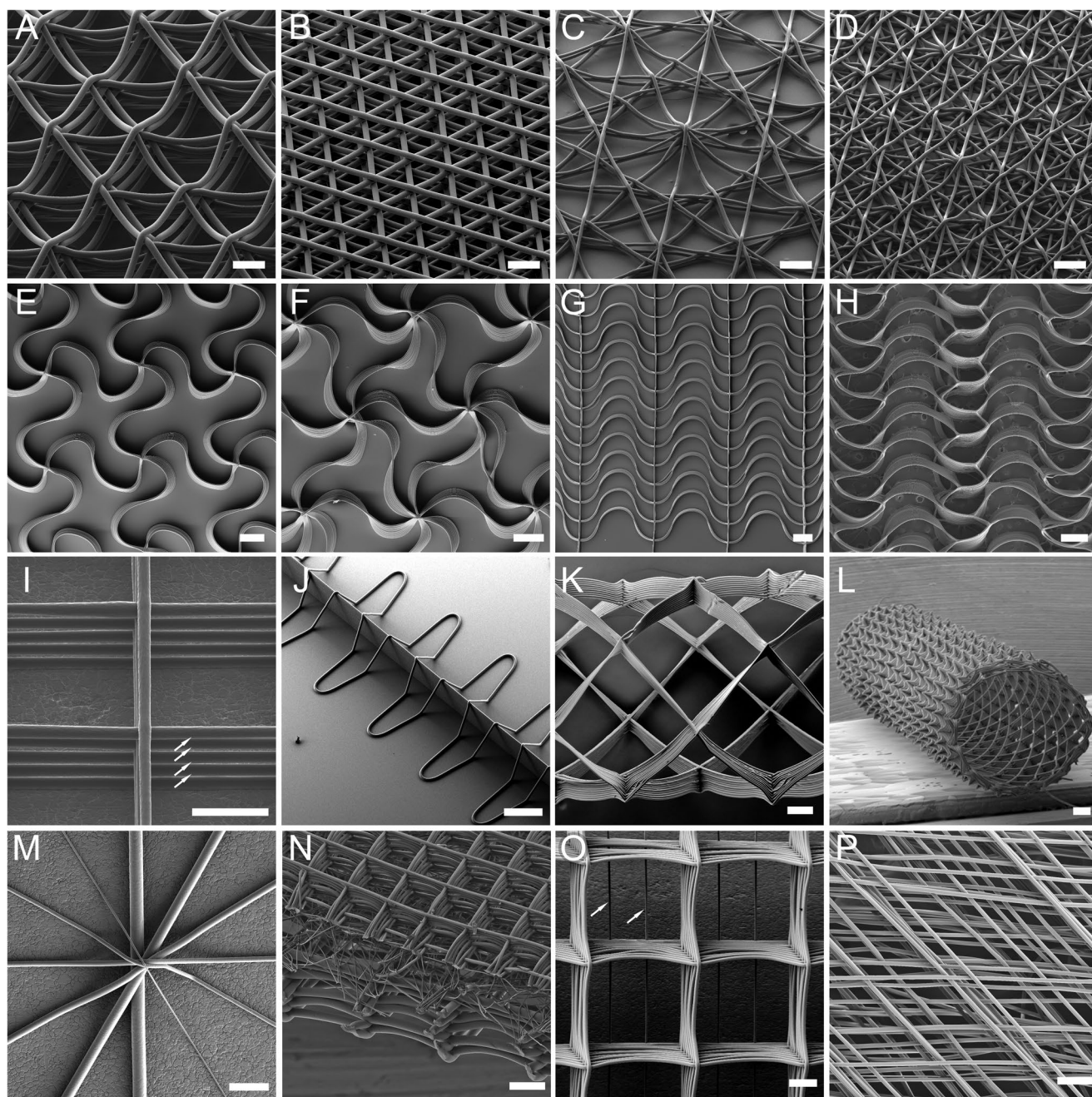
Figure 3. Scanning electron microscope (SEM) images of various melt electrowritten PCL scaffold designs. Different laydown patterns beginning with triangular/hexagon designs with A) 20 µm fibers at 250 µm spacing or B) 10 µm at 125 µm spacing, dodecagon designs with C) 10 µm fibers at 250 µm spacing or D) 20 µm at 125 µm spacing. Sinusoidal architectures with E) box and F) hexagonal designs while G) shows unidirectional and H) bidirectional structural design. I) Image of nonsagging fibers with small spaces between pores (white arrows), J) out-of-plane fibers, a highly ordered 3 mm diameter tubular scaffold with K) eight and L) 30 pivot points. M) An image of different diameter fibers crossing over at a single point. N) Shows a multiphasic scaffold design made up of three different porosity scaffolds. O) Shows a standard lattice scaffold with the addition of spheroid supporting fibers. P) A lattice scaffold design with each γ-direction staggered by 50 µm forming larger channels through the depth of the scaffold. Scale bars = 100 µm A–D), 500 µm E–H), 50 µm I), 200 µm J–L), and 100 µm M–P). A–D) Reproduced under the terms and conditions of the Creative Commons CC BY-NC-ND 3.0 License.[29] Copyright 2019, The Authors, published by Mary-Anne Liebert. E–G) Reprinted with permission.[30] Copyright 2017, American Chemical Society. H) Reproduced with permission.[31] Copyright 2019, Wiley. I) Reprinted with permission.[32] Copyright 2019, Elsevier. J) Reproduced under the terms and conditions of the Creative Commons CC BY-NC-ND 3.0 License.[26] Copyright 2019, The Authors, published by Wiley. K–L) Reproduced under the terms and conditions of the Creative Commons CC BY-NC-ND 3.0 License from.[33] Copyright 2018, The Authors, published by Elsevier. M–N) Reproduced under the terms and conditions of the Creative Commons CC BY-NC-ND 3.0 License.[17] Copyright 2019, The Authors, published by Wiley. O) Reproduced under the terms and conditions of the Creative Commons CC BY-NC-ND 3.0 License.[35] Copyright 2019, The Authors, published by Wiley. P) Reprinted with permission.[36] Copyright 2018, Elsevier.

**ADVANCED
SCIENCE NEWS**

www.advancedsciencenews.com

**ADVANCED
FUNCTIONAL
MATERIALS**

www.afm-journal.de

mimicking the shape and mechanical properties of an ovine aortic valve leaflet and ultimately reproduce the biomechanics of a human native tissue.[31] Since the jet is a rapidly solidifying structure, there are conditions where fiber sagging predominates between intersections. This is especially observed in Figure 3A,C, while Figure 3I shows how closer placed fibers can stretch across short gaps without sagging.[32] Furthermore, de Ruijter et al. showed that out-of-plane MEW fibers could be utilized to improve the resistance to shear stress within hydrogel composites (Figure 3J).[26]

Fabricating well-defined MEW structures with an additional degree of freedom by using a rotating mandrel collector advanced over the last 5 years. The challenge of continuously direct writing a fiber on a mandrel for multiple layers was described in depth by McColl et al., who mathematically approached the design so that well-defined MEW tubes could be precisely fabricated with varying porosities and pivot points (Figure 3K–L). This research resulted in an open-access website (http://mewtubes.herokuapp.com/) that autogenerates G-codes to fabricate defined tubular MEW structures,[33] or any continuously deposited filament.

Multiphasic scaffolds are another design methodology with a future perspective within biomedical sciences, where distinct regions of scaffolds can have different porosities and architecture. Numerous publications have reported the relationship between fiber diameter and the air pressure or collector speed;[17,34] this has been visually demonstrated with a video journal publication.[16] While Hrynevich et al. used all of these factors to finely control and demonstrate a predictive level of

MEW fiber diameters during an individual print.[17] Figure 3M shows the intersecting of fibers from 5 to 30 µm in even increments. The concept of fiber diameter control is an interesting aspect regarding MEW that only adds to the infinite number of direct-writing patterns, such as MEW fibers direct-written into three distinct regions (Figure 3N). It appears that MEW will be able to provide endless variations in designs for complex multiphasic and morphologic scaffolds for various applications. After a simple calibration step, a multiphasic MEW structure with defined properties can now be printed together in a single step.[17] This is derived from better controlling and understanding of the fiber pulsing phenomenon, as discussed previously, which has significantly progressed the level of MEW scaffold designs. Other MEW scaffold approaches that have been adapted from the typical lattice laydown patterns include spheroid-holding structures[35] (Figure 3O) and staggered scaffold walls to allow improved migration of cells[36] (Figure 3P). **Table 1** lists all the currently published scaffold designs with respective MEW instrument configurations.

4. Developments in MES/MEW Devices

The notable improvements in MES/MEW devices have been achieved and reported primarily with in-house designed and built MEW printers, rather than commercially available systems. In fact, all commercial machines (Table S1, Supporting Information) have significant limitations and do not allow the user to perform cutting edge research, reflected in the low

Table 1. List of printed shapes including printer configurations and conditions, as well as resulting fiber diameter and associated mechanical properties. All designs were printed with Purasorb PC 12 unless otherwise stated. The following abbreviations are used: P (pressure), V (voltage), CD (collector distance), T (processing temperature), CS (collector speed), and FD (fiber diameter).

Print design	Dimension(s)	Nozzle diameter	FD [µm]	P [bar]	V [kV]	T [°C]	CD [mm]	CS [mm min⁻¹]	Application	Ref.
Sub-micrometer fibers	Box-structure scaffolds 15 × 15 mm²; 0°–90° altering layers; 100 µm fiber spacing	33G	817 ± 165 nm	2.8	2.9	84	1.5	5500	Bimodal or multimodal scaffolds for large volume tissue engineering structures	[27]
Different orientated laydown patterns	Box scaffold: 0°–90° Hexagon scaffold: 0°–60°–120° Octagon scaffold: 0°–45°–90°–135° Dodecagon scaffold: 0°–30°–60°–90°–120°–150°	22G	11.23 ± 0.53	0.4	4.5	73	2.5	600	High porosity/cell infiltration scaffolds	[29]
Sinusoidal/ serpentine architecture	1 mm arc diameter; 0.5 mm circumferential fiber spacing	23G	19.76 ± 1.54	2.0	6–6.5	85	4.0	280	Mechanically relevant scaffolds for HVTE	[31]
Hexagonal shape	θ = 60°; l = 400 µm size	–	–	1.0	4.5	85	3.5	270	Stretchable myocardial patch	[137]
Out of plane	A = 20–1000 µm; λ = 100–3200 µm	25G	13.30 ± 0.30	2.0	6.0	90	3.0	400	Out-of-plane stabilizing fibers	[26]
Large volume scaffold	7.1 mm at 7 kV; 6.2 mm at 8 kV; 5.7 mm at 9 kV	–	20.00 ± 1.50	–	7–9.0		8.0	–	High-volume scaffolds with uniform morphologies and fiber diameters	[12]
Precision Tubes	30-pivot points; 20° winding angle; 1.5 mm diameter; pore size 0.4 mm²	22G	18.20 ± 2.10	1.0	7.0	89	4.0	506	Controlled direct writing onto a cylinder	[33]
Stacking different porosity scaffolds	Scaffold 1: 125 µm spacing Scaffold 2: membrane mesh Scaffold 3: 250 µm spacing	22G	11.18 ± 0.40; 30.51 ± 2.42; 49.93 ± 2.62	0.5; 2.0; 4.0	8.5	73	6.0	750; 420; 300	Multiphasic scaffolds	[17]

number of publications resulting from these devices. Hence, this has given rise to a diverse and rapidly growing number of system concepts built by research groups and not industry that tackle a spectrum of challenges faced within each research application. This diversity in house-built devices has resulted in an ecosystem that has expanded our understanding of MES/MEW further. Yet it is a condition sine qua non for further broadening the application of MEW in the wider research community that a state-of-the-art commercial MEW printer is available in the near future.

4.1. Digitization of the MEW Jet

The impact of digitalizing the electrowritten jet was recently demonstrated for multiparametric analysis. The term "Printomics" was defined as the high throughput analysis of 3D printing parameters with minimal human intervention.[13] Using images of the MEW jet to provide measurements or inputs is essential to rapidly develop the best processing conditions for a range of diameters, when there are many different parameters affecting the jet (**Figure 4**). Using high-resolution imaging of the jet as a manufacturing output, closes the digital loop of inputs/outputs for the automated high throughput analysis of 3D printing parameters.[13] This digitization approach enables automated parameter control to analyze a spectrum

of printing variables in real-time. The in-process control loop allowed for an automated parameter adjustment and parallel monitoring of fiber diameter as well as the flight path of the fiber.[13] Moreover, the combination of visual data and a conveyor belt collector (Figure 4B) enables the generation of large data volumes that can be readily subjected to statistical models. The effect of parameters can therefore be defined in-depth with regard to fiber diameter (Figure 4C) and flight path. Using Printomics, the effort required for processing and formulating different polymers for MEW would be reduced.

4.2. Scale-Up Systems

From an industry perspective, scale-up is essential for MEW to increase its technology readiness level (TRL). The lengthy fabrication time for MES/MEW remains to be a barrier to progressing to the next TRL. Hence, first efforts have been undertaken to address and better translate both of these techniques to satisfactory industry manufacturing requirements.[13,37]

In general, scale-up methods for additive manufacturing can be categorized into two classes: 1) multiple individually moving print heads[13,37] and 2) multiple nozzles integrated into one print head.[38] A scale-up approach for MEW using the former class was proposed after Wunner et al. demonstrated that the influence of gravity on the jet can be effectively controlled
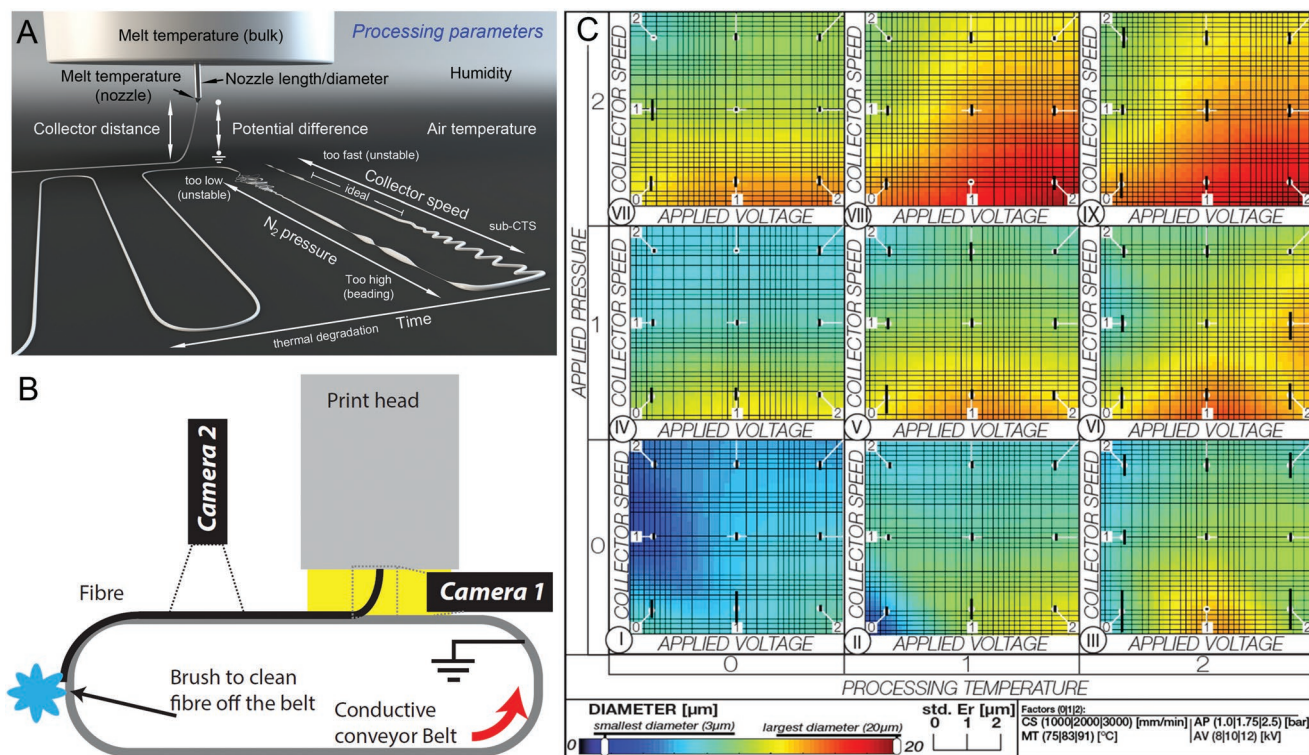
Figure 4. Digitalization of the MEW jet. A) Schematic of the MEW jet and fibers, with all processing parameters that affect print quality listed. B) A schematic of the Printomics setup for MEW where fibers are collected onto a conveyor belt, rather than an *x*–*y* collector, and constantly removed with a brush. A two-camera system is implemented to record the jet angle and fiber diameter simultaneously, resulting in the generation of large datasets for automated analysis. C) Shows an example of the high-throughput analysis with a fiber diameter heat map, depicting the influence of four key parameters (voltage, collector speed, applied pressure, and processing temperature) on diameter control.[13] A) Adapted with permission.[101] Copyright 2019, Wiley. B) Reproduced with Permission.[13] Copyright 2019, IOP Publishing.

**ADVANCED
SCIENCE NEWS**
www.advancedsciencenews.com

**ADVANCED
FUNCTIONAL
MATERIALS**
www.afm-journal.de

Figure 5. Effect of gravity on the jet and implications for scale-up. The minimal effect of gravity on the MEW jet during printing shown in A) a horizontal orientation and B) upside-down orientation followed by the translation into C) a scale-up MEW printer capable of fabricating 1024 scaffolds/print and D) a singl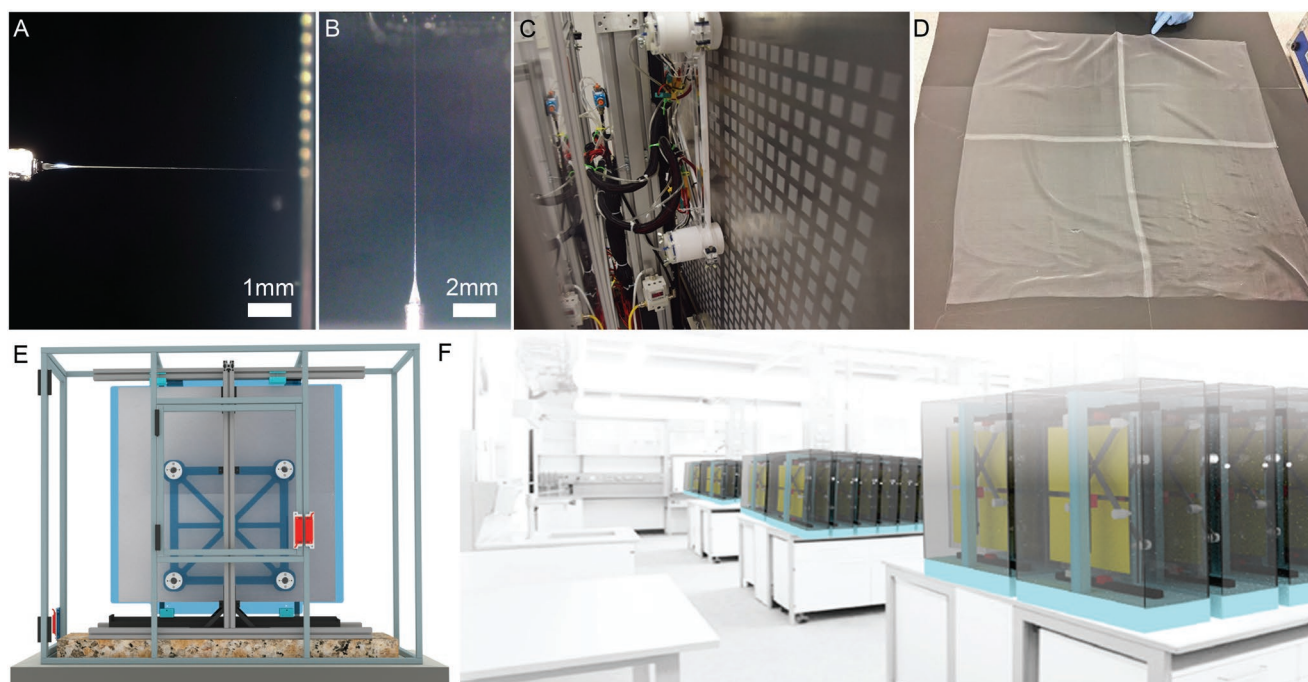e 80 cm × 80 cm fabric. E) Image showing a CAD model of the scale-up prototype configuration with 8 print heads even spaced on a horizontal configuration to a large translating collector and F) a computer rendering envisioning how the small footprint permits multiple systems operation in unison. A–B) Reprinted with permission.[39] Copyright 2018, Elsevier. D,F) Reproduced with permission.[37] Copyright 2019, Mary-Anne Liebert.

(**Figure 5**A,B) by adjusting the system parameters depending on each printing orientation of the Taylor cone (upright, sideways or upside-down configurations).[39] This opened up new avenues for MEW device design, such as one with a double-sided, vertical collector.[37] By adopting an eight-head MEW printer with a vertically configured collector (Figure 5C–F) many samples or large sheets of MEW fabric could be fabricated.[37]

A multinozzle approach within a single head has recently been advanced to total of 600 nozzles within a single head and combined with a conveyor belt system for MES.[40] The distance of deposition becomes larger when the working distance and needle spacing increases and this improves control of the MES process.[41] While it has been described that a multi-head strategy is particularly an essential component for MEW scale-up,[4] increasing the nozzles within a head is an essential part will greatly impact both MES and MEW output. Other scale-up approaches have already been proposed including the manufacturing of submicron fiber yarns by a needleless MES processing with the assistance of suction wind and rotating collection for industrial-scale production.[42]

4.3. Dynamic Electric Fields

Two major factors are known to be responsible for insufficient electrostatic forces when building voluminous MEW scaffolds. The most common being the deflection of fibers from their vertical trajectory, which arises from the accumulation of charges within the top most layers of scaffolds and prevents new

upcoming fibers from linear stacking.[12,43] These insulating fibers result in the exposed collector regions being more electrostatically attractive for emerging molten fibers. The second major factor that leads to insufficient electrostatic forces is the discussed fiber pulsing behavior and the formation of large droplets/beads, which can occur when the print head moves out of the applied voltage working zone. While it is important to set a low voltage initially for dynamic electric fields, it must also be sufficient enough to avoid fiber pulsing.[11,12]

A third lesser-described factor that influences the fabrication of voluminous MEW scaffolds includes the fiber breaking of the upmost layers. These often-sagging fibers create a spanning gap across which a fiber lifts back toward the charged nozzle/head due to the presence of a strong electrostatic field and proximity to a heat source.[12] When a sufficient amount of kinetic energy is subjected onto these fibers, a breaking event occurs, disrupting the regularity of the printed structure. Such misplaced material disrupts the electric field, and fiber accuracy in later layers will be affected; it is especially problematic at large build heights.[12]

A number of systems have been described using either a positive charged nozzle and a ground collector, or a dual voltage power supply, where a positive voltage is placed on the needle tip and a negative voltage on the collector plate.[6] The latter demonstrated to increase the maximum number of layers for each construct considerably, more recently it has been shown not to be the case. Wunner et al. established that the build height for precise MEW scaffolds can be significantly increased with an increasing electric field while maintaining the nozzle to object distance,[12] resulting in voluminous MEW scaffolds with

**ADVANCED
SCIENCE NEWS**

www.advancedsciencenews.com

**ADVANCED
FUNCTIONAL
MATERIALS**

www.afm-journal.de

distinct channels. While also demonstrating that the lowest initial charge will generate the most nondistorted layers and result in thicker MEW scaffolds.[12] Adopting this approach for MEW (and also MES) is predicted to greatly expand the design possibilities for the respective technologies, facilitating the fabrication of large constructs with well-defined architecture and high resolution.[44]

4.4. Spinneret and Nozzle Design

As demonstrated in 2010 by Zhmayev, the nozzle size plays a significant role in the final straight jet diameter.[45] Experiments have evolved from the simple nozzle configuration, as Esmaeilirad et al. examined the effects of different nozzle-exit-channel shapes (circular, square, triangular, etc.) on PCL fiber diameter[46] while Morikawa et al. demonstrated an interesting MES technique in which a wire is used, producing fibers with a significantly lower diameter.[47] This method is different from conventional MES methods, which typically rely on jet drawing via standard nozzles.

With the recent interest in scaling-up production to industrial standards, a number of MES nozzle designs and configurations have been investigated. Yang and colleagues[38,48] previously introduced "needleless" MES systems that were described as having umbrella-like or cone-shaped nozzle. More recently, these needleless MES devices have continued to show use in the production of ultrafine poly(lactic acid) (PLA) fibers for application toward the treatment of marine oil spill pollution.[49] Chen et al. demonstrated this technique, combined with air suction, flowing air was used to direct as many as 80 jets from a single spinneret resulting in a cluster of melt electrospun fibers.[50] By further combining this needless MES method with a rotating collection substrate, the continuous manufacturing of nanofibers yarn has been shown and suction wind speed identified as an important parameter when accessing ultrafine fiber diameters.[42] An alternate approach in the same vein, has been proposed for the mass production of polymer melt jets ejected from burst bubbles, termed bubble MES, and collected onto a grounded substrate.[51] This method ultimately utilizes the needless approach of the environmentally friendly technique of MES to fabricate uncontrolled polymer fibers ranging from thick to thin microscale in diameter.

To date, numerous research groups have been focused on exploring a suitable and efficient way to produce coaxial MES for microencapsulation and controlled release of growth factors and drugs,[52] vascular regeneration,[53] and resistive sensing devices[54] while obvious potential applications include soft robotics[55] and wearable textiles.[56] Two methods have arisen as current alternate routes for coaxial MES. Lee et al. demonstrated the fabrication and characterization of MES microfibers with encapsulated structures using electrically heated melt coaxial electrospinning and compared these to melt-blending microfibers.[57] In turn the coaxial structure demonstrated a significant increase in strength while PCL blended microfiber sheets were brittle upon tensile testing. The second approach generates quasicore/sheath microfibers from compressed poly(3-hydroxybutyrate-*co*-3-hydroxyhexanoate) (PHBH)/poly(L-lactic acid) (PLLA) strips via laser-melting MES.[58]

4.5. Laser Heating

In the mid-2000s, Ogata and colleagues established the use of CO_2 lasers to heat a solid filament for MES.[59] A polymer sample is locally heated with a spot like laser beam, and resultant fibers directed toward a collector by an electrostatic field. The idea being an MES method that utilizes less energy compared to conventional approaches, in addition to not requiring organic solvents when compared to SES. With more researchers attempting to improve MES, several groups have investigated laser heating as an energy source. Recently, Xu et al. demonstrated chemically stable and microscale diameter cellulose fibers via laser-heating MES.[60] Suzuki et al. used CO_2-laser supersonic drawing method to fabricate poly(ethylene terephthalate) (PET) nanofibers followed by compression-molding to obtain a cylindrical 3D structure suitable for tissue engineering applications.[61] A laser heating MES approach is the preparation of layered polymer films to fabricate patterned fibers. For example, Fujii et al. demonstrated core (EVOH)-clad polypropylene (PP) nanofibers and hollow PP nanofibers fabricated from PP/EVOH/PP three-layer films using a line-like CO_2 laser-beam MES system.[62] Xu et al. fabricated PHBH/PLLA quasicore/sheath microfibers by using a CO_2 laser system producing mechanically relative textiles.[63] Finally, Asai et al. studied the influence of the structure and piezoelectricity of poly(vinylidene fluoride) (PVDF) fibers processed by linear laser-MES and further compared the results with conventional SES. The results indicate that crystallinity of MES fibers was comparable between the two techniques.[58] To date, it can be seen that the technique of MES is evolving leading to considerable improvements to device and/or apparatus design, which opens the door to new horizons in processing fibers.

4.6. Combinatorial Manufacturing Processes

The combination of MEW with other manufacturing technologies is a logical next step to add design perspectives to the final product. This approach was employed after previous research showing an exponential increase in mechanical strength when MEW fibers were combined within a weak hydrogel.[15] This led to the combination of extrusion-based 3D bioprinting with MEW as demonstrated by de Ruijter et al. in a single-step biofabrication process.[64] A 3D bioprinter with a charged collector plate for MEW arranged cells/bioink and fibers in a spatially arranged manner (**Figure 6**).

4.7. Miscellaneous Approaches

In general MES, when compared with SES, has advantages such as environmental friendliness due to lack of solvent evaporation in the processing, low costs and suitability for various polymers, in particular for polymers without a suitable solvent at room temperature.[5,65] However, many researchers describe MES as restrictive due to involving complex apparatus with extra heating system, especially for an electrical heating system, which may involve electrostatic interference during the MES process.[65a,66] Despite this, Yan et al. was able to demonstrate
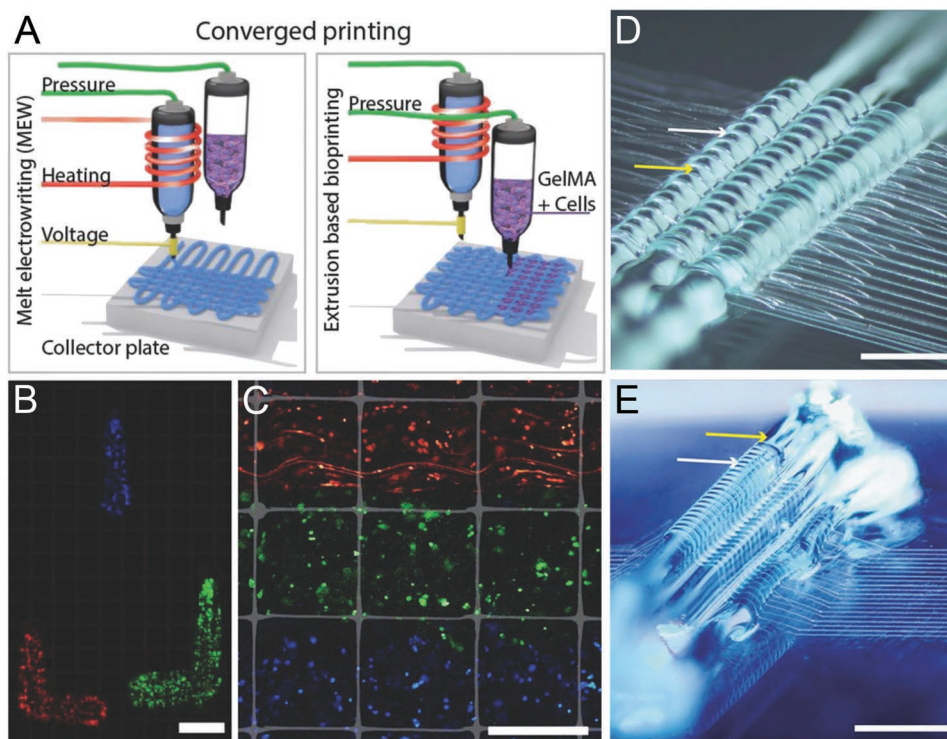
**ADVANCED
SCIENCE NEWS**

www.advancedsciencenews.com

**ADVANCED
FUNCTIONAL
MATERIALS**

www.afm-journal.de

Figure 6. Combination of MEW processing method with extrusion-based 3D bioprinting. A) An illustration of MEW and extrusion-based bioprinting combined into a single-step approach resulting in the fabrication of B,C) porous constructs via MEW followed by the spatial placement of cell-laden hydrogels inside respective scaffold pores. The selected embryonic mesenchymal stem cells individually stained with with DiI (red), DiO (blue), or DiD (green). The fabrication of MEW fibers combined with hydrogel (Pluronic, 40% w/v) to guide more complex fiber arrangements, including D) inter-locked with hydrogel strands and E) built out-of-plane with stacking of hydrogel strands. Yellow arrows are used to show hydrogel and white arrows indicating the MEW fibers. Scale bars = 400 μm B,C) and 500 μm D,E). Reproduced under the terms and conditions of the Creative Commons CC BY-NC-ND 3.0 License.[64] Copyright 2019, The Authors, published by Wiley.

the proof of principle of a portable electrospinning apparatus based on a solar cell and a hand generator which could process both MES and SES for different kinds of polymers.[67] This portable MES setup approach was further expanded by combining an alcohol lamp with a candle/lighter as heating system and a hand generator associated with high-voltage converter.[66] Similarly, Qin et al. demonstrated melt electrospun PCL and PLA fibers by using a hand-operated Wimshurst generator.[68] These efforts to design an MES device that allows easy setting up and without extra power supply needed are examples that these techniques can be made accessible. Recently, consumer-grade 3D printers that typically fabricate rigid plastic have seen modification to support MES for desktop usage by hobbyists.[69] The incorporation of MES into these settings provide new opportunities for fabricating interactive objects and sensors that combine the flexibility of MES textiles with constructs of rigid plastic for actuation, sensing and tactile experiences. These include, but not limited to, an origami-style folding lamp with piezoresistive brightness control, an actuating plastic flower that opens when textile liquid sensor detects sufficient water in the soil, and interactive media that responds to capacitive sensing via a melt electrospun textile.[69]

Researchers have also modified first generation MEW devices for different purposes. For example, Ko et al. adapted an MES device to include a small-scale microcompounder that fed PCL filaments directly into the melt chamber of the printing head.[70]

A potential technique for rapid investigation of different polymer blends, directly from compounding to melt electrospun fibers. Mayadeo et al. utilized a volumetric heat source placed downstream of the jet to provide further thinning of fibers. This was also supported by a nonisothermal Giesekus constitutive model.[71] An integrated gas-assisted MES device with a hollow disc electrode concept was introduced, where Liu et al. showed that the molten jet could proceed through and elongate.[72] This demonstrated a new method of obtaining ultrafine melt electrospun fibers without using a grounded collector.

5. Polymers

The number of polymers being processed by both MES and MEW has gradually expanded over the last five years. Application-specific technologies drive this trend to utilize the advantages of MES and MEW over other polymer processing technologies.

5.1. MES

MES generally forms random-type fibers, similar to solution electrospinning, flash spinning and jet blowing, due to the electrical instabilities within the jet.[4,9] An overview of the
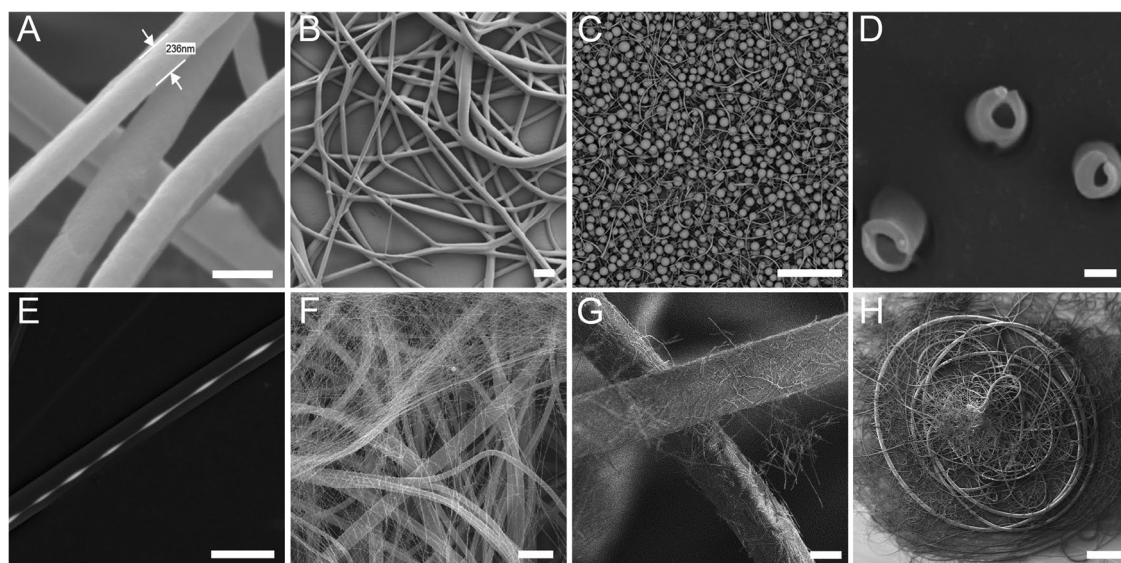
**ADVANCED
SCIENCE NEWS**
www.advancedsciencenews.com

**ADVANCED
FUNCTIONAL
MATERIALS**
www.afm-journal.de

Figure 7. Various MES scaffolds and print designs. A) PLA nanofibers melt electrospun with the assistance of airflow. B) Polymer melt fibers of PLA ejected via bubble MES. C) Beaded and microsphere fibers fabricated with PLA with exceeding 250 °C. D) Cross-section of PP/EVOH/PP layer films melt electrospun resulting in hollow fibers. E) Optically active fibers using hybrid perovskite microcrystallite material. F) PVA/PP composite fabricated by a combination of MES and SES. G) TiO$_2$ fibers combined with melt electrospun polyamide fibers. H) melt electrospun PEEK fibers. Scale bars = 500 nm A), 100 µm B,C), 1 µm D), 10 µm E), 20 µm F), 10 µm G), and 500 µm H). A) Reproduced with permission.[76] Copyright 2018, Wiley. B) Reproduced under the terms and conditions of the Creative Commons CC BY-NC-ND 3.0 License from.[51] Copyright 2018, The Authors, published by Elsevier. C) Reproduced with Permission.[77] Copyright 2018, IOP Publishing. D) Reproduced with permission.[62] Copyright 2018, Wiley. E) Reproduced with permission.[79] Copyright 2018, Materials Research Society. F) Reproduced with permission.[80] Copyright 2014, Wiley. G) Reprinted with permission.[81] Copyright 2019, Elsevier. H) Reproduced with permission.[94] Copyright 2019, Wiley.

characteristics of nonwoven fibers in general can be found elsewhere.[73] **Figure 7**A–H shows notable melt electrospun fibers that were published within literature. Correspondingly, **Table 2** lists the polymers recently processed via MES with respective parameters and settings. The MES process of PLA fibers has been further optimized using an orthogonal design method by Doustgani et al., reporting an average fiber diameter of less than 100 nm[74]—currently the smallest diameter MES fiber reported. To achieve these dimensions, the fibers were made using gas-assisted melt electrospinning (abbreviated to "GAME"),[75] and were regular in diameter and homogeneous in morphology.[74] Air flow was also used by Qin et al. to reduce the diameter of PLA fibers down to 236 nm (Figure 7A).[76]

König et al. altered the electrical conductivity of PP via the addition of sodium stearate and sodium oleate as well as an antistatic additive, to establish a more uniform diameter distribution.[40a] It was further shown that sodium stearate with Irgastat attributed to an increase in electrical conductivity leading to the fabrication of nanofibers. Li et al. reported polymer melt jets ejected from burst bubbles collected on a grounded substrate,[51] and shown in Figure 7B. Yu et al. showed that when the temperature of PLA melt exceeded 250 °C, beaded fibers and microspheres (Figure 7C) were produced.[77] These PLA melts would become gradually decomposed and molecular chains would break, resulting in a reduced entanglement degree and PLA microfibers exhibited beaded and microsphere morphology.[77] Zaiss et al. explored a different approach by allowing fiber coiling from a static position above a textured, metallic dome collector to produce open pore morphologies.[78] These MES meshes, which resemble the

pattern on the dome, resulted in a scaffold with a convex and concave-shaped architecture on the upper side and underside, respectively.

A PP/EVOH/PP three-layer films has also been melt electrospun using a line-like CO$_2$ laser-beam MES system and images from cross-sections are shown in Figure 7D showing a hollow feature.[62] Optically active fibers using hybrid perovskite microcrystallite material have been fabricated via MES shown in Figure 7E.[79] Combining PHBH was also reported with PLA, to increase the processability of PHBH and the mechanical properties of PLA, and specifically how they form from sandwiched strip at the tip of Taylor cone to quasicore/sheath microfibers, respectively, by using the technique of laser-heated MES.[63] Some researchers have sought to combine SES and MES to form polyvinyl alcohol (PVA)/PP membranes (Figure 7F) for enhanced water filtration properties.[80] Sidaraviciute et al. combined fibrous titanium dioxide (TiO$_2$) on melt electrospun polyamide fibers (Figure 7G), to increase the efficiency of the immobilization of TiO$_2$ against organic pollutants.[81] Other recent polymers processed by MES include reduced tungsten oxide nanoparticles dispersed into a PLA melt and formed into a membrane with enhanced light-driven water evaporation performance for potential applications in water treatment and desalination.[82] Short MES fibers were produced from small molecules based on cyclic butylene terephthalate.[83] Li et al. optimized parameters for melt electrospun fibers of an inorganic–organic hybrid material, poly(dimethylsilylene ethynylenephenyleneethynylene) (PMSEPE), which were cured after a two-step reaction resulting in enhanced thermal stability and high mechanical properties.[84]

ADVANCED
SCIENCE NEWS
www.advancedsciencenews.com

ADVANCED
FUNCTIONAL
MATERIALS
www.afm-journal.de

Table 2. Melt electrospun polymers including parameters/conditions. The following abbreviations are used: *P* (pressure), *V* (voltage), CD (collector distance), *T* (processing temperature), CS (collector speed), and FD (fiber diameter).

Polymer/blend	Description(s)	Nozzle diameter	Processing temperature [°C]	Feed rate	V [kV]	CD [mm]	CS [mm min⁻¹]	FD [µm]	Ref.
PVDF	Poly(vinylidene difluoride); piezoelectric polymer	26G	190	1.5 bar	2.70	4	–	17–55	[101]
pHMGCL/PCL	Poly(hydroxymethyl-glycolide-*co*-ε-caprolactone)/poly(ε-caprolactone)	27G	84	2.0 bar	5.0	3	300	4–7	[34b]
PUS	Poly(urea-siloxane)s; thermoplastic elastomer	24G	90	2.0 bar	10.0	8.5	2500	10–20	[14]
PP	Polypropylene	25G	215	0.5 bar	6.2	3.3	750	16.4 ± 0.2	[97]
P(LLA-ε-CL-AC)	Poly(ʟ-lactide-*co*-ε-caprolactone-*co*-acryloyl carbonate)	30G	145	3.0 bar	7.0	4.5	420	24.6 ± 2.7	[95b]
PLA–PEG–PLA/PLA/45S5 BG	Polylactide-poly(ethylene-glycol) blends with 45S5 bioactive glass particles	23G	142	2.0 bar	4.0	3.5	5000	31 ± 2	[99]
WO₂.₇₂/PLA	Reduced tungsten oxide/polylactic acid	–	260	0.013 g min⁻¹	4.0	–	100 rpm	8–13	[82]
PP/EVOH	Polypropylene/poly(ethylene-*co*-vinyl alcohol)/polypropylene	–	CO₂ laser; 50 W cm⁻²	4.0 mm min⁻¹	20–70	100	–	0.88 ± 0.30	[62]
PLLA-PHB	Poly(ʟ-lactic acid)/poly(3-hydroxybutyrate)	–	220	–	35	70	–	10.60 ± 2.5	[129]
PHBH-PLLA	Poly(3-hydroxybutyrate-*co*-3-hydroxyhexanoate)/poly(ʟ-lactic acid)	–	CO₂ laser; 3 W cm⁻²	400 µL h⁻¹	18	50	–	9.99 ± 1.4	[63]
CBT	Cyclic butylene terephthalate oligomer	–	190	–	20	150	–	1.8–2.6	[83]
PLA/ATBC	Poly(lactic acid)/acetyl tributyl citrate	–	240		40	90	–	0.23–1.75	[76]
PLA/starch/PCL/nHA	Polylactic acid/starch/poly(ε-caprolactone)/nanohydroxyapatite	20G	180	50 µL h⁻¹	20	100	–	45–65	[131]
PS/DCJTB/PE	Polystyrene/4-(dicyano-methylene)-2-tert-butyl-6(1,1,7,7-tetramethyl-ljulolidyl-9-enyl)-4H-pyran/polyethylene	18–23G	240	Gravity feed	15	50	–	80	[98]
PMSEPE	Poly(dimethylsilylene ethynylenephenyleneethynylene)	–	150	Gravity feed	35	50	–	5–45	[84]
PCL/HAp	Poly(ε-caprolactone)/hydroxyapatite	21G	80	20 mL h⁻¹	7	10	–	16.84 ± 2.41 (3 wt%) 20.46 ± 1.09 (7 wt%)	[114b]
PA6	Polyamide-6; magnesium, calcium and zinc additive	17G	250	1.5 mL h⁻¹	135	450	1.5–2 rpm	–	[89]
PA12	Poly(amide-12)	8.5G	300	1.6 g h⁻¹	20–25	40	–	–	[81]
PEEK	Poly(ether–ether ketone)	20G	350–375	–	10	36	–	1.5–8.5	[94]
PPS	Polyphenylene sulfide	9G	315	5 mL min⁻¹	30	95	–	7.69	[184]
PPS/PP	Polyphenylene sulfide/polypropylene	–	320	–	45	80	–	4.12 ± 1.05	[182]

Xu et al. studied the self-layering of ultrafine PET fiber webs, where the melt electrospun fibers laminated into thirteen concentric layers.[85] Nazari et al. have continued to investigate the MES ability of PLA/polyethylene glycol (PEG) blends, by defining the critical concentration of PEG phase segregation and confirming miscibility at the interfacial interaction using rheological parameters.[86] Furthermore, they demonstrated that PEG would alter the melt viscosity and increased the polarity of the jet.[87] Ko et al. combined melt electrospun PCL with sugar particles to induce porous microfibers.[88] Malakov et al. showed that the use of magnesium, calcium and zinc stearates combined with polyamide melt electrospun fibers

resulted in smaller diameters due to a decreased viscosity and increased electrical conductivity.[89] Singer et al. demonstrated that trisamides could be melt electrospun into supramolecular fibers. Also showing that bisamides and sorbitols mainly result into microspheres while perlene bisamides form well-defined fibers due to strong π–π interactions.[90]

Reduced tungsten oxide (WO₂.₇₂) nanoparticles were included into a PLA melt and formed into a membrane with enhanced light-driven water evaporation performance for potential applications in water treatment and desalination.[82] PHBH was also combined with PLA, to increase the processability of PHBH and the mechanical properties of PLA, and

**ADVANCED
SCIENCE NEWS**

www.advancedsciencenews.com

**ADVANCED
FUNCTIONAL
MATERIALS**

www.afm-journal.de

form sandwiched strips by using the technique of laser-heated MES.[63]

Lastly, the unique characteristics of PEEK, such as its high thermal and chemical resilience, make it a desirable engineering material in a wide variety of applications. These include filtration membranes as separators in fuel cell applications,[91] gas separation[92] or in aerospace applications.[93] Recently, Govinna et al. established melt electrospun unsulfonated fibers of poly(ether ether ketone) (PEEK) (Figure 7H) without the reduced thermal stability and chemically altered PEEK fibers which typically occurs with SES.[94] This important development could replace the need for aggressive solvents and avoid sulfonation, which is destructive to the properties of PEEK.

5.2. MEW

There have been several polymers that have been processed via MEW for the first time since our previous review.[4] This includes commercially available PP and PVDF, as well as polymers specifically synthesized for MEW processing, such as (AB)$_n$-type segmented copolymers,[14] UV photo-crosslinkable polymers[95] and PCL-based blends.[34b] Thermoplastic polymers are generally chosen for melt processing since they can be made easily pliable and malleable above a specific temperature which further solidifies upon cooling.[11] Specifically, these polymer chains interact through intermolecular forces, which weaken rapidly when an increased temperature is applied, yielding a viscous liquid and able to be utilized to produce microscale fibers with high control. Most thermoplastics typically have a high molecular weight thereby increasing the degree of chain entanglement that is required to create a jet at the low mass flow rates required for MEW. From a processing perspective polymers such as poly(urea-siloxane) (PUS) have shown to be excellent alternatives.[14] This (AB)$_n$-type segmented copolymer based on soft and hard segments of siloxane and urea respectively forms supramolecular cross-links at room temperature. Interestingly, fiber fusion that occurred at the intersections lead to no fiber sagging and effectively similar build height across the top of the scaffold.[14]

Hochleitner and co-workers improved the MEW-processing of a UV photo-crosslinkable poly(L-lactide-co-ε-caprolactone-co-acryloyl carbonate) poly((LLA-ε-CL-AC))[95b] by removing the lactide component, resulting in (PCL-co-AC).[95a] Not only did fiber placement improve, the thermal stability and lower processing temperatures for PCL-co-AC also expanded the allowable processing time for this thermally degrading polymer. By UV crosslinking the MEW-processed structures, the modulus of the hydrated scaffold was greatly improved, and resistant to dynamic loading. Sub-micrometer diameter MEW fibers based on PCL were achieved by using conditions that minimize flow rate and maximize the electric field—these distinct conditions can be found in Table 1.[27] Haigh et al. demonstrated the controlled deposition of MEW fibers for PP; the MES of PP onto static collectors had been previously reported.[48,96] Interestingly, PP required a heated collector that enabled the production of linear fiber arrays, stacked fibers and porous materials.[97] In contrast to commercial fused deposition modeling (FDM)

printers, where heated collectors are standard, most MEW do not require heated collectors.

For MEW, PCL remains the gold standard,[11,17] in particular for tissue engineering applications due to its slow degradation rate.[98] A comprehensive list of all the recently reported polymers and their variants that have been melt electrospun to date is included in Table 2. Castilho et al. showed the addition of a hydroxyl group (−OH) to PCL, giving poly(hydroxymethylglycolide-co-ε-caprolactone) (pHMGCL), which improved the degree of cellular alignment on MEW scaffolds.[34b] Hochleitner et al. reported that the addition of 45S5 bioactive glass particles to PLA–PEG–PLA triblock copolymers showed to be a promising polymer/ceramic composite for stimulating bone tissue formation.[99]

Piezoelectric polymers are suitable for numerous applications such as flexible electronics, soft robotics, tactile sensors, energy harvesters, acoustic transducers and inertial sensors.[100] Florczak et al. established MEW processing conditions for PVDF, a well-known polymer with electroactive properties, demonstrating that fiber deposition can be highly controlled, enabling the fabrication of precise complex 3D structures.[101] These fibers attained their piezoresponse sufficient for use in sensing applications[101] while the demonstration of actuating potential remains to be described. As previously described in the laser heating section, Asai et al. demonstrated MES processing to produce PVDF fibers and compared the structure and piezoelectricity with conventional SES process.[58] Moreover, measurements revealed that the crystal structure of MES fibers was mainly alpha phase, whereas the SES fibers showed higher a beta phase fraction. It was also found that the crystallinity of MES fibers was comparable to that of SES.

5.3. Surface Coatings

Another approach to enhance polymer function includes surface coatings. These are often employed to provide greater enhancement over the control of cellular function, and/or adhesion by attaching bioactive or inorganic molecules to the surface of the submicron fiber scaffolds. Delalat et al. utilized surface coatings of anti-CD3 and anti-CD28 antibodies covalently bound to the MEW scaffold, fabricated with medical-grade PCL, to convert the 3D lattice to a human T cell expansion platform.[102] Paindelli et al. demonstrated PCL scaffolds fabricated by MEW and coated with calcium phosphate (CaP) coating engendered osteogenic maturation when seeded with human mesenchymal stem cells (MSCs) along osteogenic medium.[103] This engineered platform enabled a bone-mimetic environment for probing the therapy response and underlying mechanism of resistance of cancer cells. Similarly, Hammerl et al. fabricated MEW scaffolds with PCL and used a surface coating of CaP which were further cultured with osteoblasts (OB) and peripheral blood mononuclear cells to make a growth factor-free coculture system.[104] The use of CaP coating, for example, better mimics the physiological microenvironment of the regenerating bone niche and can be applied for the screening of scaffolds' bone regeneration potential.[105] Others have used cell adhesion and antibodies to enhance cell growth along the fiber network. Recently, Bertlein et al. demonstrated

1904664 (13 of 28)

**ADVANCED
SCIENCE NEWS**

www.advancedsciencenews.com

**ADVANCED
FUNCTIONAL
MATERIALS**

www.afm-journal.de

that the post-modification of PCL scaffolds obtained with MEW via sP(EO-stat-PO) coating provided a protein repellent and a more biocompatible interface due to increased surface hydrophilicity.[106] Alternatively, Lee et al. utilized a poly(ethylene dioxythiophene) (PEDOT): polystyrene sulphonate (PSS) coating on a nonconductive elastic fibers that are melt electrowritten with polyether block amide. The coated microstructured thin film enabled a conductive surface and high sensitivity for use as resistive sensors.[54]

5.4. Fugitive Inks

New methods utilizing fugitive inks have also been investigated. Haigh et al. demonstrated that indirect printing of PCL templates via MEW within poly(2-oxazoline) hydrogels is a feasible method to produce highly defined hierarchically structured hydrogels within 3D porous channels (**Figure 8**).[107]

PCL MEW scaffolds were fabricated (Figure 8A), embedded within a poly(2-oxazoline) hydrogel (Figure 8B), solubilized with a solvent exchange (Figure 8C) and then placed within a fluorophore to demonstrate the channels (Figure 8D). The precise channels can be seen due to localized fluorescence (Figure 8E), which permeates into the hydrogel with time (Figure 8F). This technique is used in biosensor development, drug delivery, and certain biomedical and tissue engineering applications, to tune diffusion and transport of nutrients and growth factors.

Kotz et al. described a method to fabricate arbitrary embedded freeform 3D-suspended hollow microstructures in transparent fused silica glass with a sacrificial template replication process,[108] outlined in Figure 8G–I. PCL microfiber meshes (Figure 8J) were produced by MEW and immersed in a nanocomposite, which was consecutively processed to decompose and evaporate polymeric residue and to give fused silica glass microstructures (Figure 8K).
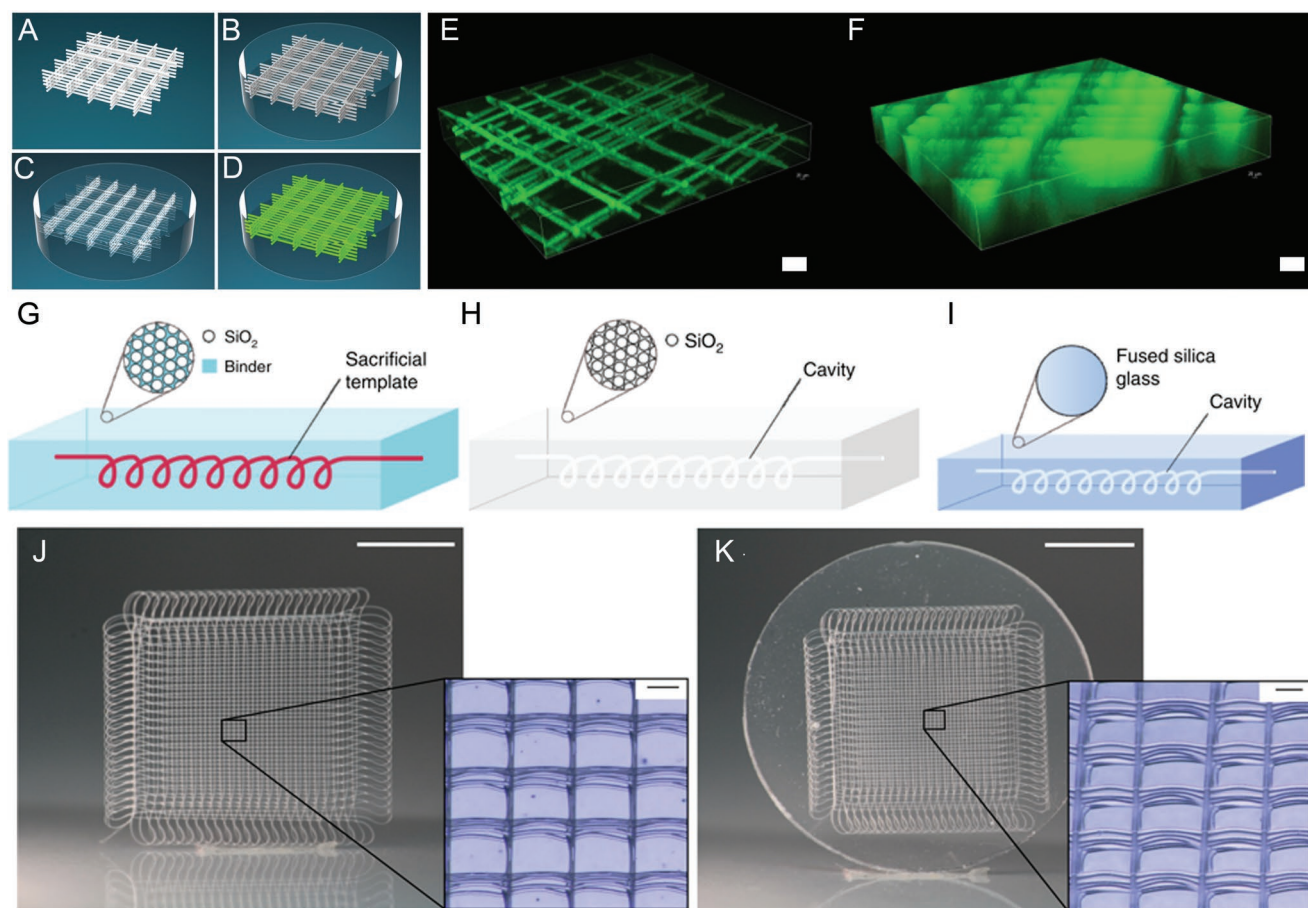

Figure 8. MEW fugitive ink strategies. A rendering of the sacrificial template method within a hydrogel, where A) the PCL template (white) is printed via MEW and then B) embedded in the hydrogel. The empty channels C) within the hydrogel are further generated after solubilizing the PCL, before backfilling with D) a fluorescein dye. E) Shows the time-dependent diffusion of FITC-dextran through the channels after 5 h and F) from the channels into the hydrogel after 22 h. A sacrificial template method can also be used to form suspended hollow microstructures within fused silica glass material. G) A polymeric scaffold is embedded into an amorphous silica nanocomposite followed by H) thermal debinding and I) sintering into fused silica glass. J) Shows an example MEW lattice made from PCL with the thermal de-binding process removes the polymeric template resulting in K) an inverse hollow lattice structure in fused silica glass via sintering. Inset image showing the series of microcavities remaining. Scale bars = 100 µm E,F), 5 mm (inset: 100 µm (J–K)). A–F) Reproduced with permission.[107] Copyright 2015, Wiley. G–K) Reproduced under the terms and conditions of the Creative Commons CC BY-NC-ND 3.0 License.[108] Copyright 2019, The Authors, published by Nature Publishing.
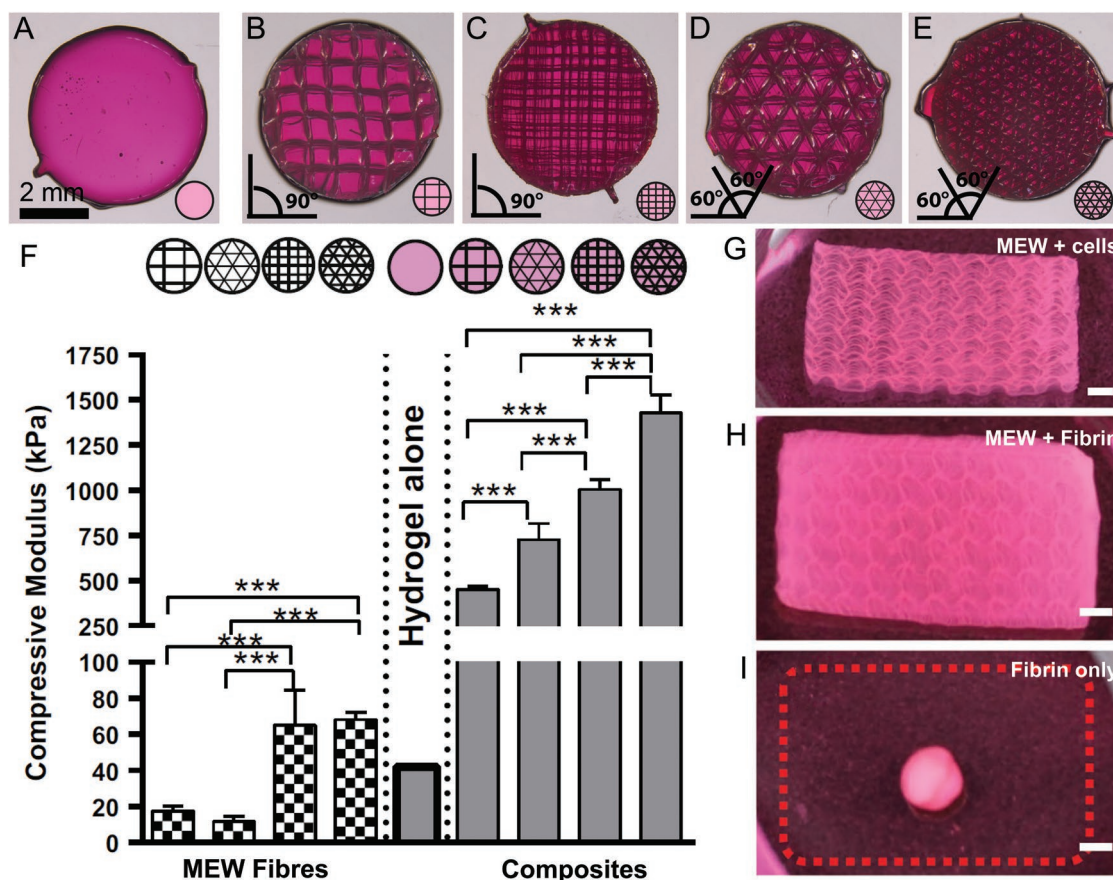
ADVANCED
SCIENCE NEWS
www.advancedsciencenews.com

ADVANCED
FUNCTIONAL
MATERIALS
www.afm-journal.de

Figure 9. Different MEW–hydrogel composite strategies. MEW pattern reinforcements within gelatin methacrylamide (GelMA)/hyaluronic acid methacrylate (HAMA) hydrogels, with A) hydrogel alone, B) 0°–90° pattern and 800 µm pores, C) 0°–90° pattern and 400 µm pores, D) 0°–60°–120° pattern and 800 µm pores and E) 0°–60°–120° pattern and 400 µm pores.[111] F) Shows the aforementioned MEW pattern designs and their compression modulus alone and inside a GelMA/HAMA hydrogel. Sinusoidal MEW scaffolds support the G) seeding of cells and H) embedding of fibrin, both images taken after a two-week period. I) The contraction that non-reinforced fibrin undergoes when similarly cultured for two weeks. The dashed line indicates the original size of the fibrin. Scale bar = 2 mm G–I). A–F) Reproduced with permission.[111] Copyright 2015, Elsevier. G–I) Reproduced with permission.[31] Copyright 2019, Wiley.

5.5. Soft Network Composites

Soft network composites have been fabricated from a variety of different manufacturing technologies, mainly for improvement of structural integrity and strength.[109] MEW reinforcing structures are defined as mechanical metamaterials, which have nonuniform mechanics.[110] A combination of a hydrogel and reinforcing MEW network made of medical-grade PCL (**Figure 9**A–E), has been used in several studies.[30,34a,111] MEW fibers are used for 1) alternative reinforcing strategies to toughen soft hydrogels and 2) facilitate cellular proliferation and alignment along fibers that mimic the extracellular matrix (ECM) microenvironment.

The remarkable aspect of MEW-reinforced hydrogels is that individually, the matrix and scaffold have low mechanical properties (Figure 9F). When combined, they form a significantly stronger soft network composite with mechanical properties up to 50 times greater than their individual designs. Furthermore, this reinforcement effect occurs at ultralow polymer volume fraction (up to 97% porosity) of the MEW fiber network.[15,111] The laydown pattern, e.g., whether the fiber is sinusoidal or linear, also influences the mechanics, as shown in Figure 9A–F. In another

reinforcement perspective, MEW fibers prevent fibrin from contracting after multiweek culture periods (Figure 9G–I).[31]

In order to meet the intricate requirements of each native human tissue, a significant proportion of MEW literature aims to provide a high level of both biological and mechanical functionality. Recently, there has been a number of developments into tailoring these precisely controlled soft network composites for biomedical applications, including highly organized scaffolds that withstand the anisotropic reversible deformations of the heart;[31,34b,112] multiphasic composites that mimic articular cartilage[15,34a,113] and bone;[114] as well as multiscale theoretical modeling to predict the mechanical behavior.[34a,115]

Bas et al. reported a computational study performed where a numerical model was used to predict the design of a most biomechanically suited scaffold to reflect multiphasic zonal features of articular cartilage.[34a] A multiphasic scaffold combined with a medical-grade PCL/hydroxyapatite nanoparticles (nHA) biomaterial was selected and fabricated to mimic the cartilage calcified zone, which was further embedded into a crosslinked hydrogel solution. This pilot study further resulted in being a comprehensive in silico design library to assist the selection of

**ADVANCED
SCIENCE NEWS**

www.advancedsciencenews.com

**ADVANCED
FUNCTIONAL
MATERIALS**

www.afm-journal.de

suitable fiber–hydrogel network designs for TE applications; in order to reduce time, cost and efforts dedicated to fabrication and experimental testing of potential scaffold designs.[34a] In addition to improving the compressive strength of hydrogels de Ruijter et al. showed that out-of-plane MEW fibers (Figure 3J), specifically intended to stabilize an existing structure improve the shear modulus of hydrogel–fiber composites.[26]

The mechanism of reinforcement for such fiber–hydrogel composites was investigated with a mathematical approach, and a multiphasic scaffold was developed based on numerical modeling.[30] The fundamental reinforcement mechanism of these microfibers within hydrogels has been detailed by Castilho et al., using both a continuum FE model based on experimental scaffold geometry and µCT images of the construct geometry during compaction.[116] The mechanical properties of the fiber–hydrogel composites are governed by two distinct mechanisms. These include fibers in tension by lateral expansion of the hydrogel as well as the load transfer through fiber cross-section interconnections with each dominating the reinforcement depending on low or high fiber volume fraction, respectively. Bas et al.[30] and Chen et al.[115] used mathematical approaches to describe fiber–hydrogel composites via multiscale and homogenization theoretical modeling. This provided an in-depth account of the effective material properties of the composite, given parameters of the constituent materials, and the geometrical arrangement of the fibers and hydrogel. This mathematical modeling approach is an important step and as more data is added, an in-depth in silico design library can be expanded for different MEW scaffolds partnered with soft hydrogel material that can be closely related to specific tissue application.

5.6. Hybrid/Solution 3D Direct Writing

There is an increasing overlap in the technologies of solution EHD direct writing and MEW, where the former uses a polymer solution at room temperature instead of a melt.[117] Logically, the boundaries between solution EHD direct writing and MEW are blurred and there are examples of EHD direct writing from heated polymer solutions. This was done in two instances to decrease the viscosity; the first for PCL and strontium-substituted bioactive glass to make the printing solution sufficiently extrudable.[118] Similarly, water has been used as a plasticizer to lower the processing temperature, to reduce degradation of the polymer or incorporated drug. Semjonov et al. recently demonstrated the MES of PCL-PVAc-PEG/indomethacin (IND) fibers via the simple addition of water in a controlled manner lowering the temperature significantly thereby preventing drug degradation.[119]

Small diameter fibers made by EHD have applicability in a range of applications similar to MEW.[120] Often, both SES and MEW are attempting to address attributes that the other one dominates in. Only through careful process design, optimization and control, sub-micrometer fibers can be obtained in MES/MEW, while they are readily made with SES. Conversely important advances for the controlled placement of fibers has recently occurred for solution EHD direct writing[117b] although they currently do not match the resolution or build height of MEW.

6. Applications

Since MES/MEW results in materials with a high aspect ratio of surface to volume, the potential applications are similar to that for SES. They include filtration,[121] textiles,[62] water evaporation and desalination,[82] flexible electronics and resistive sensors,[54] soft robotics,[30] as well as scaffolds for tissue engineering,[26,30] biofabrication,[122] and cancer research.[123] This section aims to highlight the state of the art for applications for both MES and MEW.

6.1. Drug Delivery

Different drug delivery methods have been studied all throughout literature,[124] each have described the need for controlled drug release systems, where sustained and/or boosted drug release can be exhibited over a defined period of time, relating to such applications as drug-loaded implants,[125] and wound dressings[126] for adequate long-term effects. Since many drugs possess poor water solubility, they often require enhanced dissolution to achieve sufficient bioavailability.[119] Furthermore, drug loading in traditional electrospun fibers is often limited by the solubility of the drug and the solvent concentration in the mixed solvent system. Melt processing, on the other hand, can be utilized for a drug with poor water solubility and benefit from an improved release.[52] In addition, a major advantage is the 3D-woven mats or nonwoven meshes that can be finely tuned with chemical components, such that different geometric structures and number of layers are more distinct in directly controlling drug release behavior.[127] These techniques are aimed to control the overall drug release mechanisms, ultimately for pharmaceuticals, leading to several research groups to explore the use of MES and MEW for tailored drug delivery therapies. A comprehensive list of all MES/MEW fibers with reported processing methods and composite variants for drug delivery applications to date is detailed in **Table 3**. In terms of drug release, Cao et al.[128] and Liu et al.[129] explored melt electrospun fiber meshes of PLA/polyhydroxybutyrate (PHB) with different concentrations of the drug dipyridamole. In addition, demonstrating that an increase in PHB can be used to depress the PLA crystallinity degree and significantly increase the rate of short-time drug release.

Similarly, Lian et al. showed drug-loaded PCL fibrous membranes, resulting in a slow drug release rate and a long-term release period.[130] Antibacterial compounds are a particularly attractive class of drugs since they can be used within a wide range of medical applications, especially tissue engineering where functional cells are attempted to be grown inside soft hydrogels. This has led to antibacterial blends being optimized for MES, for example, Davachi et al. established an optimized interface-modified antibacterial blend based on PLA/PCL/starch melt-mixed with nHA and triclosan.[131] When seeding of fibroblast (L929) cells on such melt electrospun fibers revealed a desirable drug release and antibacterial properties. Furthermore, the combined use of nHA alongside the encapsulated triclosan demonstrated the ability to eliminate the adverse effects of the antibacterial drug.[131] Alternatively, Rahman et al. demonstrated a coextrusion technique where

Table 3. Melt electrospun fibers for drug delivery applications. The following abbreviations are used: *P* (pressure), *V* (voltage), CD (collector distance), and FD (fiber diameter).

Polymer blend(s)	Drug	Processing temperature [°C]	V [kV]	CD [mm]	Geometric structure/ pore shape	FD [μm]	Application(s)	Ref.
PLLA/PHB	Dipyridamole; antithrombotic/ antithrombogenic	170	35	70	Nonwoven mesh	18.8 ± 6.0	Short-time drug delivery	[128]
PLA/starch/PCL	Triclosan; antibacterial	180	20	100	Nonwoven mesh	45–65	Hard and soft tissue engineering; drug delivery	[131]
Soluplus	Indomethacin; nonsteroidal anti-inflammatory	180	10	50	Nonwoven mesh	300–400	Drug delivery; tissue engineering	[119]
PCL/PEG	Ciprofloxacin; antibiotic	150	5	–	Square grid; tri-angles; rhombuses	42–136	Wound dressing; tissue engineering; drug delivery	[127]
PCL	Daunorubicin; antitumor agent	90	30	150	Nonwoven membrane	2.5 ± 1.6	Chemotherapy; drug delivery; tissue engineering	[130]
PEG	Draconis sanguis, borneol, red dan and musk (black plaster; herbal)	80	40	80	Nonwoven membrane	17.8 ± 9.4	Transdermal patches and skin irritation	[133]
PCL	*Rosmarinus officinalis* L.; antimicrobial extract	80	20	50	Nonwoven mesh	–	Bioactive packaging; antimicrobial coating	[134]
PP/HDPE	Chlorohexidine dihydrochloride; antibacterial	210	–	–	Composite fibrous tapes	2.0 ± 0.6	Antibacterial membranes	[132]

an antibacterial additive (CHDH) was melt electrospun within a PP and high density polyethylene (HDPE) blend in order to make PP/CHDH/HDPE composite fibrous membranes.[132] Demonstrating highly efficient antibacterial characteristics, He et al. demonstrated via MEW the preparation of PEG/PCL/ Ciprofloxacin (Cip) composite fiber mats with different PEG/ PCL ratio. Consequently, the release of the drug could be controlled by adding PEG and changing the geometric structures from square-shape grid to triangular to rhomboidal.[127] With this added control it allows for the preparation of different type of wound dressings and dosage of drugs according to specific injury sites or illness. PEG has also been used to deliver herbal formulations for transdermal patches and to reduce skin irritation.[133] Bhullar et al. additionally utilized the nontoxic and environmentally friendly MES technique for the fabrication of antimicrobial microfibrous structures for bioactive packaging.[134] A natural antimicrobial additive was combined with PCL to inhibit microbial growth in the packaging industry, such as food and healthcare.

6.2. Biomedical Applications

Biomedical science applications have been a key driver on the frontier of MEW technology development in recent years. While additive manufacturing of polymer melts into scaffolds is primarily applied to hard tissues, MEW provides avenues for soft-tissue tissue engineering applications such as cartilage,[15] skin,[135] periosteum,[114a] nerves[136] and cardiac tissue.[34b] As previously outlined, the recent advancements of fiber–hydrogel composites and surface coatings in particular have enabled the use of MEW fibers to tackle several biomedical challenges. In 2002, the National Cancer Institute announced a new thrust "Signatures of the Cancer Cell and Its Microenvironment" with an annual budget of $40 million. A significant aspect of this initiative is the adoption of 3D culture technologies to better

recapitulate the tumor microenvironment. Based on this program, a shift has begun to take place in both the cancer research community and funding agencies that support tumor biology as to the relative importance of microenvironmental control in differentiation and cancer. This effort has led to the development of complex human tissue models to study the effects of chimeric antigen receptor T-cell therapy (CAR-T), chemotherapeutics and cancer progression.

6.2.1. Fiber-Reinforced Matrices

As highlighted earlier, the combination of MEW fibers and hydrogels gives more control over the mechanical microenvironment of the cell. For example, Castilho et al. designed MEW cardiac patches with well-ordered, injectable hexagonal MEW microstructures to support high tensile strains when placed on a contracting heart[137] (**Figure 10**A,B). Such a hexagonal scaffold design can absorb and release energy when deformed in the elastic regime and exhibited biaxial deformation more suitable for supporting contracting human induced pluripotent stem cells-derived cardiomyocytes (iPSC-CMs).[137] Moreover, the clinical model as well as technique for a noninvasive placement was further demonstrated on a beating porcine heart (Figure 10A–D). Saidy et al. utilized MEW technology to biomimetically design and fabricate a scaffold for heart valve tissue engineering with micrometric features similar to that of a native heart valve leaflet.[31] Furthermore, demonstrated that when embedded into fibrin and sutured into a silicon aortic root a functional representation for a native heart valve was possible (Figure 10E–G). Both of these studies highlight the great potential of MEW when combined with a biomimetic design strategy for the manufacture of scaffolds for cardiac repair applications.

As previously mentioned, 3D in vitro techniques are intended to provide a better representation of the natural cellular microenvironment than conventional 2D systems.[138]
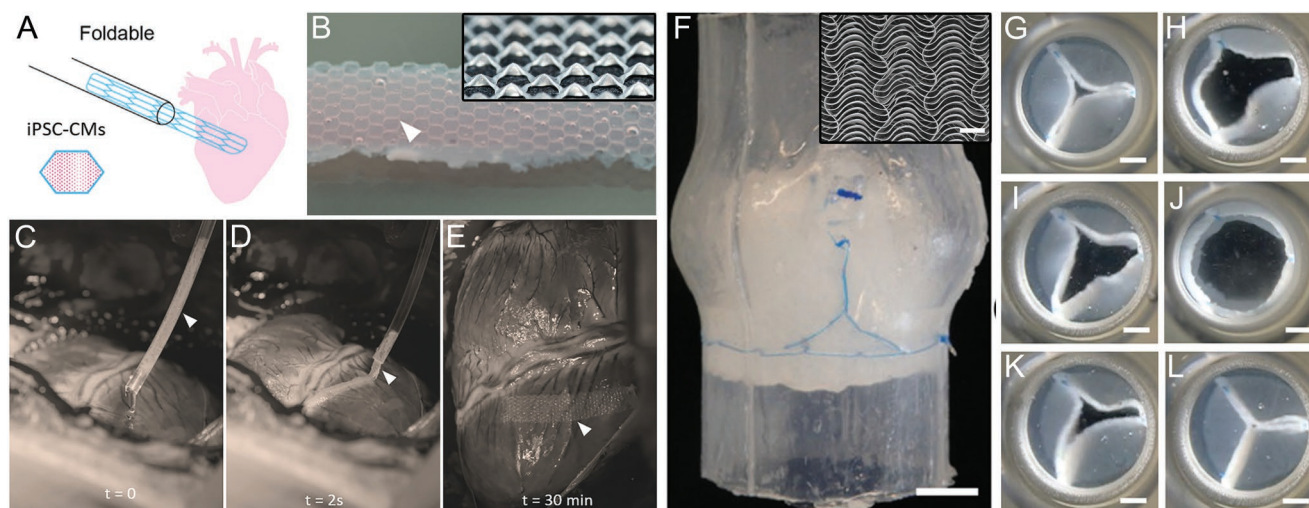
**ADVANCED
SCIENCE NEWS**

www.advancedsciencenews.com

**ADVANCED
FUNCTIONAL
MATERIALS**

www.afm-journal.de

Figure 10. Recent cardiac tissue engineering applications. A) An illustration showing the working principle of applying iPSC-CM-seeded cardiac patch directly onto functioning heart. B) Stereomicroscope image of MEW scaffold with hexagonal pattern (white arrow) indicated and inset showing a lateral view of the MEW scaffold. C,D) Photographs of the cardiac patch administration via cannula and E) the final placement of a cardiac patch on beating porcine heart. F) MEW scaffold sutured into a silicone aortic root and an inset image of the serpentine pattern used. The valve functioning in a flow loop system captured with high-speed camera shows G–L) the opening and closing sequence via the aortic perspective. Scale bars = 5 mm F–L), 1 mm F, inset). A–E) Reproduced with permission.[137] Copyright 2019, Wiley. F–L) Reproduced with permission.[31] Copyright 2019, Wiley.

Transferring measurement techniques into the 3D environment also becomes an important issue. Reflecting this, Schäfer et al. established a 3D electrophysiology approach using MEW scaffolds to reinforce Matrigel, combined with a glycine receptor-transfected Ltk-11 mouse fibroblast cell line.[139] The MEW scaffold reinforcements were shown to not interfere with electrophysiological measurements and therefore the agonist efficacy and potency of glycine receptor transfected cells in a 3D matrix was demonstrated for the first time.[139]

6.2.2. Single Cell–Fiber Studies

An essential aspect of tissue engineering is the capability to control cell function, which has led to a range of developments of scaffolds that induce natural cell morphologies.[140] For example, Eichholz et al. demonstrated that fiber–cell biophysical cues defined by MEW scaffolds could drive human stem cell behavior independent of biochemical signals.[36] This makes use of the highly aligned fiber orientations of MEW for more distinct control of cell mechanobiology and tissue specific behavior (**Figure 11**A) when compared to more randomly organized fibrous scaffolds such as those made by electrospinning. More recently, this important biophysical property has been investigated within a machine learning-based metrology platform to determine the effects of substrate architectures on cell shape and focal adhesion protein distributions via large multidimensional datasets.[141]

Additive manufacturing has brought a level of defined design control[142] that promises to deliver information-driven analysis[143] such as proteomics[144] and cell metrology.[141] Such single-cell analysis of MEW scaffold/cell interactions converges with tissue engineering digitization. For example, Tourlomousis et al. successfully combined the modeling of single-cell confinement states using confocal fluorescence microscopy, and

an automated single-cell image data analysis workflow to classify cell shape phenotypes, through quantitative metrics of the whole cell and subcellular focal adhesion protein features.[141] Figure 11B shows the cell morphology of representative neonatal human dermal fibroblasts at defined locations within a 0–90° and 0–45° MEW substrate in addition to the classifier design and accuracy evaluation result for the binary classification task. All classes corresponding to the flat or electrospun SES substrates were combined against the MEW substrate resulting in a classification accuracy level around 93%. This constitutes to MEW substrates having improved control over significant features that the machine-learning algorithm used for the classification task compared to other SES substrates. The metrology and classification confirm that pore architecture and the induced cell shape phenotypes are linked, demonstrating how bioinformatics-guided additive manufacturing can be applied to MEW. This publication has several implications, particularly the use of machine learning to analyze individual cell-scaffold interactions within a single sample.

6.2.3. Monoculture Studies

In vitro studies based on proliferation of a single cell type remains the most common form of tissue engineering approach in which MEW scaffolds are used. From these experiments, similarities in morphological formation appear to mirror those of FDM scaffolds.[145] For example, with box pore scaffolds, cell adhesion of an osteoprogenitor cell line is primarily at the corners of box-pore scaffolds and proliferation results in smooth circular structures (Video S2, Supporting Information). As proliferation and ECM deposition continues, these pores become filled and confluent with cells (Video S3, Supporting Information). As shown in Figure 11C,D, this type of cell growth follows a regular pattern seen in numerous in vitro studies.[32,34b,36]
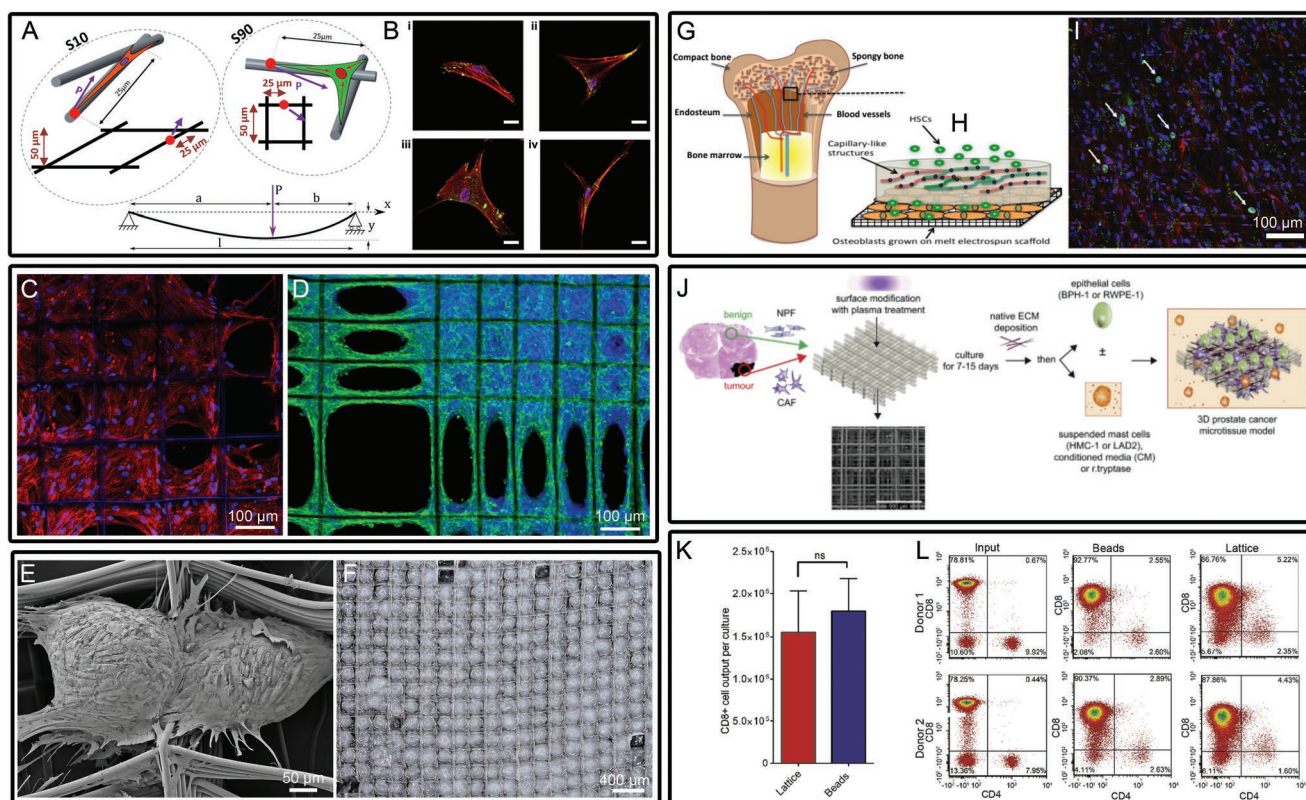
Figure 11. In vitro approaches for MEW within tissue engineering and cancer research. A) and B) show how studying the individual cell on an MEW substrate provides information on the mechanobiology and response to the microenvironment. C) and D) demonstrate how proliferating cells form C) circular or D) oval formations depending on the geometry. E) is an SEM image of two adipose-derived spheroids in adjacent pores and F) a photograph of a transferable sheet containing hundreds of spheroids. G) and H) are schematics of coculture systems that are intended to recapitulate the stem cell niche while I) is a fluorescent image of the construct with arrows indicating CD45+ and CD34+ cells that attached and migrated into hOB seeded scaffolds using osteogenic conditions. J) is a schematic of a 3D cancer model established using MEW scaffolds, while panels K–L) show how MEW scaffolds are equivalent to bead cell culture which is a mainstay of CAR T-cell therapies. Scale bars = 20 µm. A) Reprinted with permission from.[36] Copyright 2018, Elsevier. B) Reproduced under the terms and conditions of the Creative Commons Attribution 4.0 International License from.[137] Copyright 2018, The Authors, Nature Publishing. C) Reproduced under the terms and conditions of the Creative Commons CC BY-NC-ND 3.0 License from.[51] Copyright 2018, The Authors, published by IOP Publishing. D) Reprinted with permission.[32] Copyright 2019, Elsevier. E–F) Reproduced under the terms and conditions of the Creative Commons CC BY-NC-ND 3.0 License.[35] Copyright 2019, The Authors, published by Wiley. G–H) Reprinted with permission.[155] Copyright 2017, Elsevier. I) Reprinted with permission.[154] Copyright 2017, Elsevier. J) Reprinted with permission.[158] Copyright 2019, Elsevier. K–L) Reprinted with permission.[102] Copyright 2017, Elsevier.

even when the MEW scaffold is adhered to a nonadhesive substrate.[27]

Variations exist with different pore geometries, such as with rectangular pores with high degree of cellular alignment along the rectangular shape scaffold long axis (Figure 11D).[32,34b] For example, Nguyen et al. found that instead of circular pores, rectangular pores fill with cells to create an oval-shaped space where the time to fill is related to the fiber spacing (Figure 11D).[32] Additionally, pHMGCL/PCL polymer blends with a rectangular-organized fiber architecture exhibit broad mechanical properties similar to that of native myocardial tissue.[137]

Using square-pore MEW scaffolds, Fuchs et al. demonstrated osteoblast adhesion and proliferation in a pilot study[147] for application in guided bone regeneration in oral and maxillofacial surgery. With similar square architectures, Weigand et al. showed how breast mesenchymal cells proliferated and filled an MEW scaffold in a similar, rounded, manner.[148] Human MSCs also formed such rounded pores when cultured on 80 and 150 µm square pores made from sub-micrometer

diameter fibers (Figure 11C).[27] Gradient and offset scaffolds, those with variable fiber placement also in the z-direction, were shown to aid in hOB infiltration and proliferation compared to standard MEW scaffolds.[105]

Mohtaram et al. combined both MES and SES to demonstrate how topography can be used to differentiate human iPSC-derived neural progenitors into neurons as well as direct neurite outgrowth.[149] Similarly, Kim et al. combined MES/SES methods to produce silk fibroin/PCL composite scaffolds which provided a suitable environment for human-derived MSC proliferation, adhesion and differentiation into osteoblasts during in vitro bone regeneration.[150] Kumar et al. reported a proof of concept using MEW for the designing of a biphasic scaffold that mimicked the architecture of native bone and when loaded with bone morphogenetic growth factor-2 (BMP-2) aided in vertical alveolar bone regeneration.[151] Specifically, it was shown that the biphasic construct provided biomechanical stability and long-term cell viability, some of which are crucial for vertical bone augmentation. From a vascularization perspective, Bertlein et al.

**ADVANCED
SCIENCE NEWS**
www.advancedsciencenews.com

**ADVANCED
FUNCTIONAL
MATERIALS**
www.afm-journal.de

used box-pore MEW scaffolds with cell-accumulation technology to guide the formation neovascular-like structures.[146]

Liao et al. also outlined a bilayered silicone/PCL-based scaffold using MEW, which improved cell responses for a sutureless inflow cannula.[152] Cell attachment and growth was greatly enhanced through the addition of PCL scaffolds. This proof of concept has the potential to eliminate tissue necrosis at the site of compression, to minimize thrombus formation and to restrict tissue growth to prevent inflow obstructions.

6.2.4. Spheroid Culture

Spheroids are an attractive building block for the biofabrication of tissue constructs.[153] An in vitro study combining MEW scaffolds with multicellular spheroids enabling adipogenic differentiation within sheet-like constructs was demonstrated (Figure 11E,F), where box-structured MEW scaffolds were tailored to spheroid size and further seeded with adipose-derived stromal cell (ASC) spheroids.[35] This method demonstrated no shrinkage due to the MEW scaffold support, which enabled long-term structural integrity of the spheroids. While conventional spheroid fusion of newly formed tissue is frequently reported to shrink,[35] the combination of MEW scaffolds and multicellular spheroids provides a different approach for future adipose tissue regeneration and could be related to the engineering of other implants and tissue models.

6.2.5. Coculture to Recreate a Tissue Niche

Coculture experiments have been increasingly used to better recreate conditions in vivo. Muerza-Cascante et al. reported that scaffolds designed and fabricated via MEW were able to sustain hOBs and pluripotent MSCs with characteristics of the endosteal microenvironment.[154] As summarized in Figure 11G–I, it represents the variable stages of osteogenic differentiation typically found within a developing bone matrix. These approaches also provide a 3D system that better mimics the physiological tissue environment (Figure 11G), such that, the ability to grow in all three dimensions (Figure 11H) gives better access to nutrients and suitability to describe the physiological properties of the cells used.[155]

In another example of coculture using MEW scaffolds, Wu et al. used highly aligned melt electrospun PLLA meshes cocultured with human adipose-derived MSCs and human umbilical vein endothelial cells (HUVEC) to promote in vitro tenogenic differentiation resulting in tendon grafts that mimic the native tendon tissue-like architecture, anisotropy and cell phenotype.[156] Furthermore, compared with random PLLA meshes, the ordered fibrous network better mimics the native tendon ECM structure and therefore facilitating the human adipose-derived MSC orientation, proliferation, and differentiation toward tendon fibroblasts.

6.2.6. In Vitro Tumor Microenvironments

MEW scaffolds have played a role in engineering tumor in vitro microenvironments and models of varying complexity

(Figure 11J). Lössner et al. recreated an ovarian tumor microenvironment model by combining ovarian cancer cell-laden hydrogels with mesothelial cell-layered MEW scaffolds.[157] This reproducible 3D model was used to identify several factors derived from non-malignant cells that regulate ovarian cancer cell functions such as the regulatory function of kallikrein-related peptidases and proteolytic networks contributing to cancer progression.[157] These models were designed based personalized medicine concepts can be applied to different molecular subtypes of ovarian cancer histotypes or multicellular tumor microenvironment components, such as cancer-associated fibroblasts or tumor-infiltrating lymphocytes and other tumors developing extracellular microenvironment factors suitable for crosslinking into hydrogels.

Similarly, Pereira et al. demonstrated an in vitro human prostate cancer microtissue model utilizing an MEW scaffold cultured with primary patient-derived cancer-associated fibroblasts (CAFs).[158] Using this 3D model, schematically shown in Figure 11J, it was determined that tryptase positive mast cells which are the dominant subpopulation found in human prostate cancer tissues accumulating in the distal and peri-tumoral space were the main driver for upregulating cancer related genes. The cascade of interactions between CAFs, ECM and mast cells that drive early morphological transition in benign epithelia were demonstrated.

In another microtissue in vitro model, Bock et al. investigated osteoblastic bone metastases by culturing primary human osteoprogenitor cells on CaP coated MEW scaffolds.[159] Within a 3D setting, this microenvironment was shown to be able to simulate some of the biological effects of androgen deprivation on cancer progression in bone. It can be concluded that 3D cell culture models provide a promising approach to better establish and predict the heterogeneity and efficacy of anticancer therapy.

6.2.7. CAR-T Lattices

Delalat et al. demonstrated that CD8+ T cells readily expanded using an MEW lattice scaffold which could provide activation signals upon exposure to lentivirus to increase gene expression as well as expansion in effector CD4þ T cells over bead-based activation.[102] Incorporating the lattice into a combined transduction and expansion protocol significantly reduced the manipulations and complexity associated with generating bulk CAR-T doses. This approach to cell expansion could be applied for both research and industrial T-cell expansion for immunotherapy.

6.2.8. Biomaterials

One advantage of melt processing, is its applicability and use within medical device manufacture.[1] Brückner et al. compared the fabrication of PCL scaffolds by MEW and SES to provide sufficient support for a premixed calcium phosphate cement paste.[160] Both provided a flat and flexible composite material with varied mechanical performance for the potential application for curved cranial defects. Medical-grade PCL was also melt electrowritten onto a PCL tube, to create a scaffold that improves the adhesion and was tested in an ex vivo skin model.

**ADVANCED
SCIENCE NEWS**
www.advancedsciencenews.com

**ADVANCED
FUNCTIONAL
MATERIALS**
www.afm-journal.de

Cell-seeded scaffolds had better integration than nonseeded ones or the smooth PCL tubes.[161]

In addition to direct use as a biomaterial, Farag et al. used MEW scaffolds for reinforcing human periodontal ligament cell sheets. Upon decellularization DNA removal was efficient along with preservation of ECM integrity and growth retention factors.[162] The decellularized periodontal ligament cell sheet construct was later shown to support periodontal attachment in a rat periodontal defect model.[163] These results show that the method of decellularized constructs based on MEW scaffolds have the potential to facilitate periodontal regeneration in vivo.

There are several studies involving MEW that combine both in vitro and in vivo components[114a] and implanting cell-laden scaffolds is the basis for humanized xenograft models, described later. Baldwin et al. described a novel periosteum TE concept utilizing a multiphasic scaffold design in combination with different human cell types.[114a] This demonstrated that human tissue-engineered periosteum constructs successfully recapitulated the osteogenic and vascular niche of native periosteum, and that the MEW scaffold provides a suitable in vivo environment for cellular growth.

6.2.9. Humanized In Vivo Models

Validated preclinical animal models need to be developed side by side with in vitro platforms to investigate the multicellular interactions and dynamic multistep processes involved in cancerogenesis. Hutmacher's group has previously shown that scaffold-based tissue engineering principles can be used to humanize xenograft models of tumor entities such as prostate,[164] breast,[165] and ovarian cancer.[166] MEW scaffolds are therefore a substrate from which to engineer a functionally defined humanized stroma before transplantation of human haematopoietic cells or cancer cells.

Such humanized in vivo models using MEW scaffolds have become a powerful tool to perform research on tumor metastasis.[167] At the heart of biomaterials and humanized animal models is the capability for scaffolds to form neotissue, as exampled in **Figure 12** for the formation of an ossicle.[168] MEW scaffolds are effective in this respect, and numerous studies have been published on the formation of neobone,[169] usually formed from a species separate to the animal of implantation. Once these neotissues are formed, they can be studied from
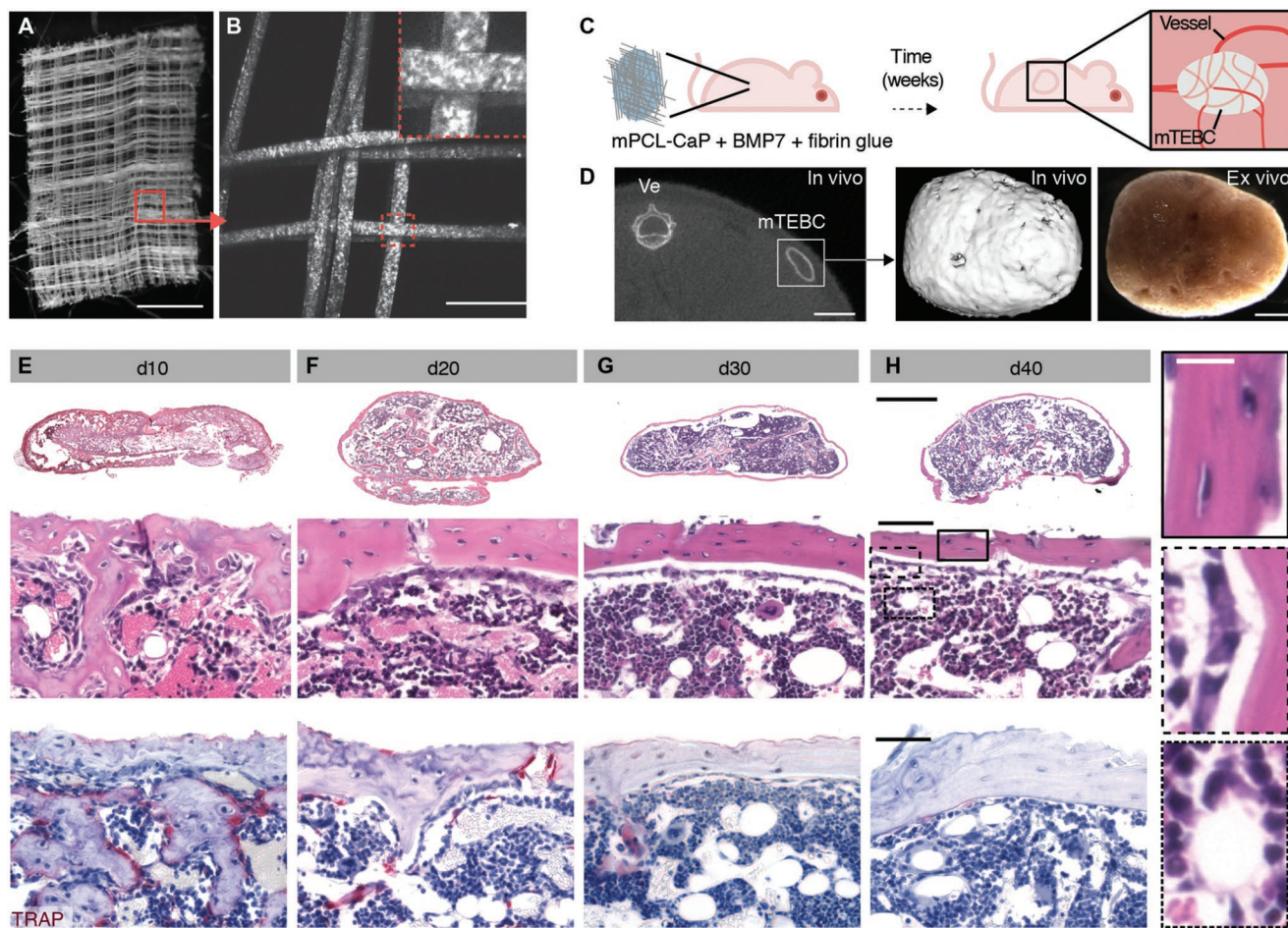

Figure 12. Example of neotissue formation of an ossicle in vivo. A box-pore CaP-coated MEW scaffold shown using A) bright-field microscopy and B) multiphoton-excited second harmonic generation. C) is a schematic showing the subcutaneous implantation of such a scaffold that is infused with fibrin glue and bone morphogenic protein 7. D) μCT and photograph of the explant after 30 days shows the ossicle tissue formation. Panels E–H) are the histology of the neotissue over various time points: 10, 20, 30, and 40 day implantation. Scale bar = 1 mm A), 100 μm B), 5 and 1 mm D), 1 mm (overview), 100 μm (insets), and 25 μm (right hand panels) E–H). Reproduced with permission.[168] Copyright 2018, AAAS.

1904664 (21 of 28)

**ADVANCED
SCIENCE NEWS**

www.advancedsciencenews.com

**ADVANCED
FUNCTIONAL
MATERIALS**

www.afm-journal.de

numerous perspectives. Figure 12A,B depicts a standard CaP-coated PCL MEW scaffold that is implanted subcutaneously to form a small neotissue. Using histology (Figure 12E–H) the progression of tissue-formation can be followed from 10 to 40 days, after which experiments can be performed, as in this case understanding of mechanisms of epithelial tumor–bone interactions and therapy response.[168]

This allows not only to test the efficacy of certain drugs against human cancer cells but also to determine their safety profile and effects on healthy human cells or tissues. As demonstrate in several studies and models, humanized organoids can be engineered and provide a humanized stroma which makes it possible to supply human transplanted cells with factors that are essential for their engraftment and proliferation. This allows investigating the behavior of human cells within their specific niches. The latter is of utmost importance as recent literature suggests that some elements of the mutual interaction between human cells and their microenvironment are species-specific. Paindelli et al. showed that metastatic prostate cancer culture in 3D osteoblastic bone stroma supports chemoresistance, consistent with in vivo studies showing that osteoblasts protect cancer cells from toxicity induced by chemo and molecular therapeutics.[103]

The Hutmacher lab was the first to develop such humanized xenograft models using MEW scaffolds[170] and subsequently published an extensive protocol to engineer humanized bone within immunodeficient mice, which can be adapted to study the interactions between human cancer cells and a humanized bone microenvironment.[123] Humanized models for breast cancer have been similarly developed.[171] Since the details of such complex in vivo studies are numerous, the reader is referred to excellent reviews elsewhere.[167,172]

6.2.10. Intravital Microscopy

For the study of fundamental tissue engineering and biomaterials aspects, in vivo studies performed with MEW scaffolds have provided live imaging insights into the immune response of implants. For example, the role of vascular endothelial growth factor (VEGF) in fibrous capsule formation and how this relates to immune cell recruitment was investigated using intravital microscopy in a so called skin chamber model.[173] In a study by Dondolossa et al. fluorescently labeled immune cells could be visualized in real time and their movements followed and quantified in real time in vivo.[173] It was determined that the excessive production of VEGF led to fibrotic capsule formation and that two different approaches that reduce VEGF production result in improved integration with the tissue. Since fibrous capsule formation is one of the greatest challenges in biomaterials, such work with MEW scaffolds provides outcomes that have broad implications for biomedical materials.

In an example of intravital microscopy applied to cancer research using humanized animal models, MEW scaffolds were CaP-coated and infused with metastatic prostate cancer cells within fibrin and BMP-7.[164] This induced osteoclast recruitment, activation, and bone resorption. There was a difference between microtumors and macrotumors in response to radium-223 treatment, with remission in the former.

Combining intravital microscopy with neotissue forming constructs is a powerful tool for metastasis and cancer research.

6.3. Soft Sensors, Flexible Electronics, and Optical Waveguides

There are numerous emerging technologies that are redefining the term "high-performance" away from traditional high-strength or wear-resistant materials. Materials are increasingly required to have optoelectrical properties *and* be flexible and resist high strain. Improvements in resolutions for 3D printing are especially being taken advantage of for flexible circuitry or optical systems.[174] As an example of this for MES, Ko et al. demonstrated utility with a femtosecond laser device for the fabrication of PCL-based stretchable force sensors for hand rehabilitation applications.[175] This technique of laser micromachining of MES fibers enables the ability to create auxetic structures within fabricated microfiber sheets, further when coated with gold particles making them conductive for sensing applications. It was shown that these sensors were sensitive and provided linear inflexion and extension in regards to strain on human skin as well.[175] Alternatively, Lee et al. developed a pressure sensor based on the PEDOT:PSS-coated microstructured thin film of polyether block amide (PEBA) (**Figure 13**A–F). PEDOT:PSS is well known for its conductivity, upon coating of melt electrowritten scaffold demonstrating a high sensor ability as well as a high sensitivity in a wide range of applied pressures. The sensitivity was further tuned by the diameter of the cylindrical microstructures of the printed film.[54]

Chen et al. demonstrated an MEW fabrication method for micro/nano-optical fibers and directly written with poly(methyl methacrylate) (PMMA).[176] It was shown that the optically active fibers have strong evanescent fields, which enable strong and rapid near-field interaction between the guide light and the analyte (Figure 13C–F), providing a reflective-index sensing with high sensitivity and fast response. This method has great potential for the direct writing of patterned optical devices and heterogeneous integrated devices.[176]

More recently, Murphy et al. reported the fabrication of optically active fiber mats via MES using a hybrid perovskite microcrystallite material.[79] Yu et al. reported an amplified spontaneous emission action within a single 4-(dicyano-methylene)-2-tert-butyl-6(1,1,7,7-tetramethyljulolidyl-9-enyl)-4H-pyran (DCJTB): polystyrene (PS) microfiber fabricated by MES.[177] This microfiber exhibited a low threshold and high gain properties, which make it an attractive candidate for organic microfibers in the field of subwavelength photonics. In addition, the single gain microfiber by MES in air enables the large-scale production of organic lasing building blocks and the full integration of coherent polymer sources in optical microsystems and disposable diagnostics.[177]

6.4. Environmental, Energy, Filtration, and Separation Applications

Governmental agencies are currently spending an increasing amount of their budget in technologies that consider the effect
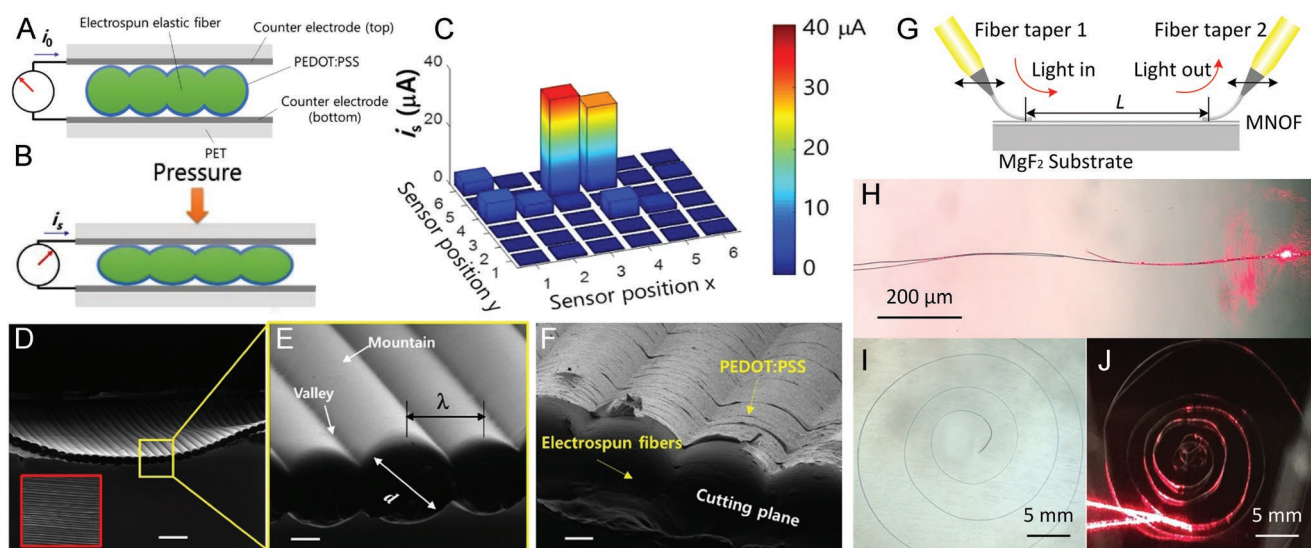
Figure 13. MEW fibers used for resistive pressure sensors and optical waveguides. General concept and schematic of an MEW pressure sensor under A) normal conditions and B) working conditions supported by C) a 3D bar graph capturing the motion of a fingertip on the surface/touch interface. D) A SEM image of an aligned MEW film and uniform fiber diameters fabricated from PEBA, inset (red border) showing a top view of the printed film. Panel (E) shows a further magnified view of the cross-section of the PEBA printed film. F) A cross-section SEM image of the MEW film depicting the polymer fibers after being coated with PEDOT:PSS. G) Schematic for the optical waveguiding of PMMA fibers fabricated via MEW using the evanescent coupling technique demonstrated with optical microscope images of a helical MEW structure and H–J) the optical characteristics under evanescent coupling. Scale bars = 50 μm D) and 5 μm E,F). A–F) Reproduced with Permission.[54] Copyright 2019, IOP Publishing. G–J) Reproduced with permission.[176] Copyright 2017, Optical Society.

on the environment, from both the manufacturing and the application perspective. Since MES/MEW is solvent-free, it falls within the general topic of green manufacturing.[178] With the rapid development of polymer materials in regard to MES, there has been increased attention to environmental filtration and green energy applications, such as water treatment and desalination, oil sorbent membranes, air filtration and separation processes. Murphy et al. demonstrated the MES of semiconducting hybrid organic–inorganic perovskite (HOIP) fibers, combined with PS to be incorporated into the pre-existing solar cell device architecture with cell lifetime sufficiently long enough to see a return on manufacturing costs.[179] Moreover, microfibers of HOIP/PS composite material prevent moisture driven degradation by encapsulation of the perovskite material in a polymer matrix with reduced chemical instability and thereby increased solar cell lifetime. This comes as performance of HOIP solid state solar cells have seen a power conversion efficiency increase rapidly from 3.81% in 2009[180] to 23.6% in 2017[181] as well as low cost of materials and ease of processing.

Alternatively, solar energy conversion is an important aspect of solar energy harvesting technologies to provide renewable, clean and sustainable energy for the development of human society. Chala et al. demonstrated an efficient MES tungsten oxide/ PLA membrane with strong near-infrared absorption capability to accelerate light-driven water evaporation for potential application in the fields of water treatment and desalination.[82] Electrospun nanofibers are widely applied in the area of water and area filtration, considered to be dominated by conventional solution electrospinning. Filtration and separation technologies have now been increasingly more accessible via the addition of MES. Serious attention has also been given to the air pollution in recent years, especially in countries with

an increased amount of fine particulate matter (<2.5 μm) in the air which is a major cause of respiratory illness.[182] Researchers have sought to combine SES and MES in designing filter membranes with good mechanical properties, high flux, and higher rejection ratio. Li et al. demonstrated this combined method by fabricating a composite PVA/PP membrane where PP was melt electrospun to act as a support layer and PVA was fabricated on the surface by SES.[80] Another approach demonstrated by Shen et al. involved the combination of MES and a hot pressing device to fabricate nonwoven PP webs with a filtration efficiency that could reach more than 95% for particles more than or equal to 2.0 μm.[182] More recently, Li et al.[49] and Bubakir et al.[121] demonstrated the large-scale fabrication of ultrafine fibrous sorbent with a high oil sorption capacity, superhydrophobicity, excellent reusability, and environmental friendliness by needleless MES using PLA and PP, respectively. This provided a new approach for the protection of aqueous ecosystems and other environmental applications. Sidaraviciute et al. reported an increase in the efficiency of the immobilization of TiO_2 by combining fibrous TiO_2 on melt electrospun polyamide fibers.[81] This composite organic-inorganic scaffold exhibited competitive structural properties and efficiency for the application in photo-catalytic degradation of organic pollutants in aqueous and airborne environments. An et al. investigated polyphenylene sulfide (PPS)/PP microfiber membranes prepared by MES as a promising high efficient material for high temperature dedusting[183] and presented a new way for the scalable and green fabrication of PPS superfine fibers. Such fibers have utility as high-strength materials.[184] Xie et al. showed a method for the MES of pure phenolic fibers and showed lower crystallization after curing as well as an increased heat resistance.[185] This has an impact for aerospace insulation materials,

**ADVANCED
SCIENCE NEWS**
www.advancedsciencenews.com

**ADVANCED
FUNCTIONAL
MATERIALS**
www.afm-journal.de

which typically use phenolic fibers due to their extraordinary flame, heat and corrosion resistance.

6.5. Microfluidics

Within the field of microfluidics there are various techniques to fabricate simple suspended hollow microstructures, the most well-known being soft photolithography. There has been recent development into utilizing the uniform diameter of melt-electrowritten fibers as sacrificial templates for microfluidic devices. From a chemical and engineering perspective, the hollow microstructures of microfluidic devices play an important role in a spectrum of applications.[186] These tend to be fabricated from a range of different materials, such as polydimethylsiloxane (PDMS) and fused silica glass, with unique geometries enabling new and advantageous physical behaviors and qualities in microfluidic devices.

Microchannels are an effective means of improving the functional performance and survival of engineered tissue analogues for regenerative medicine applications.[187] A MEW sacrificial template can be embedded into a soft UV crosslinkable hydrogel solution followed by removal during post fabrication, effectively leaving highly defined hierarchically structured hydrogels with 3D porous microchannels. For example, Haigh et al. demonstrated the successful indirect printing of sacrificial PCL templates via MEW that can be easily removed from poly(2-oxazoline) hydrogels via dissolution with an acetone-water mixture. This solvent facilitated both the dissolving of PCL while maintaining the swelling of the hydrogel to prevent distortion. The incorporation of hollow, perfusable microchannels within hydrogels for tissue engineering has attracted much attention to deliver oxygen and nutrients in hydrogels engineered for tissue engineering purposes. There remains a need to expand the materials used for fugitive inks made via MEW, similar to how other additive manufacturing technologies have advanced.[188] Fugitive ink development for MEW remains in its infancy, with PCL the current standard, which is readily removed by heat or solvent dissolution.

Zeng et al. developed a simple and cost-effective method for the fabrication of microfluidic channels based on the combination of MEW and PDMS replica-molding techniques.[189] By using MEW, microchannels with a high aspect ratio can be achieved. These are used effectively as a fugitive ink with PDMS soft lithography performed above, after bonding the respective parts. The microfluidic channels are defined by the precision and quality control of each MEW pattern. Alternatively, Kotz et al. fabricated arbitrary embedded freeform 3D suspended hollow microstructures in transparent fused silica glass by using a similar sacrificial template replication process.[108] However, instead of solvent dissolution of the fugitive ink, the hollow microstructure is generated via a thermal debinding process causing the PCL material to be passively removed.

The technique of fugitive, or sacrificial material, within MEW proposes benefits to numerous applications including, in flow-through synthesis and analysis, microfluidics, optics and photonics, tissue engineering of vascular networks and lab-on-a-chip devices.

7. Conclusions

The pace of discovery and innovation is rapidly accelerating as MES, and now MEW, fiber processing methods are increasingly embraced by the wider research community. Several other reviews mention MES/MEW,[1,44,65,110,122,136,143,190] however these lack in-depth analysis on the state of the art of both the science and technology. In this review we focus on the development within MES/MEW and distinctions within this specific field.

In recent years, the control of the jet has greatly improved, with numerous in-house built machine advancements in preventing fiber pulsing, establishment and control of dynamic electric fields as well as digitization of the jet resulting in more predictable and reproducible fiber placement. Controlling the jet from a wider range of materials beyond thermoplastic polymers will lead to further applications and is one of the next frontiers in this technology. The biomedical field will play an important role in application-driven development, especially with complex and fiber-reinforced 3D culture to elicit optimal cell behavior, while possessing the strength to withstand the specific mechanical load related to each tissue of interest.

The last few years several MES/MEW publications have focused on improving the apparatus design and detailed studies of process parameters to better obtain sub-micrometer fibers as well as increase the library of polymers that can be used. Unfortunately, industry-built machines did not implement the newest research results and are capable of only basic MEW functions.

Beyond doubt, the digitization of the jet provides the groundwork for a high-throughput system to determine complex printing parameters as well as the basis to develop an in-process control system. We anticipate that the current melt electrospinning workflow will significantly change within the next decades, as automation and stability of MEW are made straightforward and therefore putting more of an emphasis onto scaffold design for research application and/or products. It is projected that these emerging trends will expand the depth and utility of MEW/MES in an increasing number of applications in the years to come.

Supporting Information

Supporting Information is available from the Wiley Online Library or from the author.

Conflict of Interest

The authors declare no conflict of interest.

[1] A. Youssef, S. J. Hollister, P. D. Dalton, *Biofabrication* **2017**, *9*, 012002.

[2] J. Venugopal, S. Ramakrishna, *Appl. Biochem. Biotechnol.* **2005**, *125*, 147.

[3] S. Agarwal, A. Greiner, *Polym. Adv. Technol.* **2011**, *22*, 372.

[4] T. D. Brown, P. D. Dalton, D. W. Hutmacher, *Prog. Polym. Sci.* **2016**, *56*, 116.

[5] T. D. Brown, P. D. Dalton, D. W. Hutmacher, *Adv. Mater.* **2011**, *23*, 5651.

[6] N. Ristovski, N. Bock, S. Liao, S. K. Powell, J. Ren, G. T. S. Kirby, K. A. Blackwood, M. A. Woodruff, *Biointerphases* **2015**, *10*, 011006.

[7] J. He, P. Xia, D. Li, *Biofabrication* **2016**, *8*, 035008.

[8] F. Liang, H. Wang, Y. J. Li, Y. Zhou, Z. F. Wang, X. D. Chen, N. Gai, F. W. Yan, P. X. Wu, Y. B. He, Y. D. Tang, *Mater. Res. Express* **2019**, *6*, 015401.

[9] D. H. Reneker, I. Chun, *Nanotechnology* **1996**, *7*, 216.

[10] P. D. Dalton, *Curr. Opin. Biomed. Eng.* **2017**, *2*, 49.

[11] G. Hochleitner, A. Youssef, A. Hrynevich, J. N. Haigh, T. Jungst, J. Groll, P. D. Dalton, *BioNanomaterials* **2016**, *17*, 159.

[12] F. M. Wunner, M. L. Wille, T. G. Noonan, O. Bas, P. D. Dalton, E. M. De-Juan-Pardo, D. W. Hutmacher, *Adv. Mater.* **2018**, *30*, e1706570.

[13] F. M. Wunner, P. Mieszczanek, O. Bas, S. Eggert, J. Maartens, P. D. Dalton, E. M. De-Juan-Pardo, D. W. Hutmacher, *Biofabrication* **2019**, *11*, 025004.

[14] G. Hochleitner, E. Fursattel, R. Giesa, J. Groll, H. W. Schmidt, P. D. Dalton, *Macromol. Rapid Commun.* **2018**, *39*, e1800055.

[15] J. Visser, F. P. W. Melchels, J. E. Jeon, E. M. van Bussel, L. S. Kimpton, H. M. Byrne, W. J. A. Dhert, P. D. Dalton, D. W. Hutmacher, J. Malda, *Nat. Commun.* **2015**, *6*, 6933.

[16] F. M. Wunner, O. Bas, N. T. Saidy, P. D. Dalton, E. M. D.-J. Pardo, D. W. Hutmacher, *JoVE* **2017**, e56289.

[17] A. Hrynevich, B. S. Elci, J. N. Haigh, R. McMaster, A. Youssef, C. Blum, T. Blunk, G. Hochleitner, J. Groll, P. D. Dalton, *Small* **2018**, *14*, e1800232.

[18] S. W. Morris, J. H. P. Dawes, N. M. Ribe, J. R. Lister, *Phys. Rev. E* **2008**, *77*, 066218.

[19] T. Jungst, M. L. Muerza-Cascante, T. D. Brown, M. Standfest, D. W. Hutmacher, J. Groll, P. D. Dalton, *Polym. Int.* **2015**, *64*, 1086.

[20] F. Tourlomousis, H. Ding, D. M. Kalyon, R. C. Chang, *J. Manuf. Sci. Eng.* **2017**, *139*, 081004.

[21] H. Xu, M. Yamamoto, H. Yamane, *Polymer* **2017**, *132*, 206.

[22] C. B. Dayan, F. Afghah, B. S. Okan, M. Yıldız, Y. Menceloglu, M. Culha, B. Koc, *Mater. Des.* **2018**, *148*, 87.

[23] J. Ko, S. Jun, J. K. Lee, P. C. Lee, M. B. Jun, *J. Korean Soc. Manuf. Technol. Eng.* **2015**, *24*, 160.

[24] H. Ding, K. Cao, F. Zhang, W. Boettcher, R. C. Chang, *Mater. Des.* **2019**, *178*, 107857.

[25] F.-L. He, J. He, X. Deng, D.-W. Li, F. Ahmad, Y.-Y. Liu, Y.-L. Liu, Y.-J. Ye, C.-Y. Zhang, D.-C. Yin, *J. Phys. D: Appl. Phys.* **2017**, *50*, 425601.

[26] M. de Ruijter, A. Hrynevich, J. N. Haigh, G. Hochleitner, M. Castilho, J. Groll, J. Malda, P. D. Dalton, *Small* **2018**, *14*, 1702773.

[27] G. Hochleitner, T. Jungst, T. D. Brown, K. Hahn, C. Moseke, F. Jakob, P. D. Dalton, J. Groll, *Biofabrication* **2015**, *7*, 035002.

[28] J. Groll, T. Boland, T. Blunk, J. A. Burdick, D. W. Cho, P. D. Dalton, B. Derby, G. Forgacs, Q. Li, V. A. Mironov, L. Moroni, M. Nakamura, W. Shu, S. Takeuchi, G. Vozzi, T. B. Woodfield, T. Xu, J. J. Yoo, J. Malda, *Biofabrication* **2016**, *8*, 013001.

[29] A. Youssef, A. Hrynevich, L. Fladeland, A. Balles, J. Groll, P. D. Dalton, S. Zabler, *Tissue Eng., Part C*, *25*, 367.

[30] O. Bas, D. D'Angella, J. G. Baldwin, N. J. Castro, F. M. Wunner, N. T. Saidy, S. Kollmannsberger, A. Reali, E. Rank, E. M. De-Juan-Pardo, D. W. Hutmacher, *ACS Appl. Mater. Interfaces* **2017**, *9*, 29430.

[31] N. T. Saidy, F. Wolf, O. Bas, H. Keijdener, D. W. Hutmacher, P. Mela, E. M. De-Juan-Pardo, *Small 15*, 1900873.

[32] N. T. Nguyen, J. H. Kim, Y. H. Jeong, *Mater. Sci. Eng., C* **2019**, *103*, 109785.

[33] E. McColl, J. Groll, T. Jungst, P. D. Dalton, *Mater. Des.* **2018**, *155*, 46.

[34] a) O. Bas, S. Lucarotti, D. D. Angella, N. J. Castro, C. Meinert, F. M. Wunner, E. Rank, G. Vozzi, T. J. Klein, I. Catelas, E. M. De-Juan-Pardo, D. W. Hutmacher, *Chem. Eng. J.* **2018**, *340*, 15; b) M. Castilho, D. Feyen, M. Flandes-Iparraguirre, G. Hochleitner, J. Groll, P. A. F. Doevendans, T. Vermonden, K. Ito, J. P. G. Sluijter, J. Malda, *Adv. Healthcare Mater.* **2017**, *6*.

[35] R. McMaster, C. Hoefner, A. Hrynevich, C. Blum, M. Wiesner, K. Wittmann, T. R. Dargaville, P. Bauer-Kreisel, J. Groll, P. D. Dalton, T. Blunk, *Adv. Healthcare Mater.* **2019**, *8*, 1801326.

[36] K. F. Eichholz, D. A. Hoey, *Acta Biomater.* **2018**, *75*, 140.

[37] F. M. Wunner, S. Eggert, J. Maartens, O. Bas, P. D. Dalton, E. M. De-Juan-Pardo, D. W. Hutmacher, *3D Print Addit. Manuf.* **2019**, *6*, 82.

[38] H. Y. Li, H. B. Chen, X. F. Zhong, W. F. Wu, Y. M. Ding, W. M. Yang, *J. Appl. Polym. Sci.* **2014**, *131*, 40080.

[39] F. M. Wunner, J. Maartens, O. Bas, K. Gottschalk, E. M. De-Juan-Pardo, D. W. Hutmacher, *Mater. Lett.* **2018**, *216*, 114.

[40] a) K. König, F. Langensiepen, G. Seide, J. Daenicke, D. W. Schubert, *J. Nanomater Mol. Nanotechnol.* **2019**, *8*, https://doi.org/10.4172/2324-8777.1000264; b) K. König, K. Beukenberg, F. Langensiepen, G. Seide, *Biomater. Res.* **2019**, *23*, 10.

[41] H. Wang, S. Huang, F. Liang, P. Wu, M. Li, S. Lin, X. Chen, *J. Nanomater.* **2015**, *16*, 1.

[42] X. L. Ma, L. Y. Zhang, J. Tan, Y. X. Qin, H. B. Chen, W. L. He, W. M. Yang, H. Y. Li, *J. Appl. Polym. Sci.* **2017**, *134*, 44820.

[43] T. D. Brown, F. Edin, N. Detta, A. D. Skelton, D. W. Hutmacher, P. D. Dalton, *Mater. Sci. Eng., C* **2014**, *45*, 698.

[44] M. A. Heinrich, W. Liu, A. Jimenez, J. Yang, A. Akpek, X. Liu, Q. Pi, X. Mu, N. Hu, R. M. Schiffelers, J. Prakash, J. Xie, Y. S. Zhang, *Small 15*, 1805510.

[45] E. Zhmayev, D. Cho, Y. L. Joo, *Polymer* **2010**, *51*, 274.

[46] A. Esmaeilirad, J. Ko, M. V. Rukosuyev, J. K. Lee, P. C. Lee, M. B. G. Jun, *Mater. Res. Express* **2017**, *4*, 015302.

[47] K. Morikawa, A. Vashisth, C. J. Grimme, M. J. Green, M. Naraghi, *Macromol. Mater. Eng.* **2019**, *304*, 1800417.

[48] H. Y. Li, W. F. Wu, M. M. Bubakir, H. B. Chen, X. F. Zhong, Z. X. Liu, Y. M. Ding, W. M. Yang, *J. Appl. Polym. Sci.* **2014**, *131*, 40080.

[49] H. Li, Y. Li, W. Yang, L. Cheng, J. Tan, *Polymers* **2017**, *9*, 3.

[50] H. B. Chen, H. Y. Li, X. L. Ma, W. L. He, J. Tan, W. M. Yang, *Fibers Polym.* **2016**, *17*, 576.

[51] Y. M. Li, X. X. Wang, S. X. Yu, Y. T. Zhao, X. Yan, J. Zheng, M. Yu, S. Y. Yan, Y. Z. Long, *Polymers* **2018**, *10*, 1246.

[52] Z. K. Nagy, A. Balogh, G. Dravavolgyi, J. Ferguson, H. Pataki, B. Vajna, G. Marosi, *J. Pharm. Sci.* **2013**, *102*, 508.

[53] H. H. Yuan, J. B. Qin, J. Xie, B. Y. Li, Z. P. Yu, Z. Y. Peng, B. C. Yi, X. X. Lou, X. W. Lu, Y. Z. Zhang, *Nanoscale* **2016**, *8*, 16307.

[54] G. Y. Lee, H. T. Lee, W. Ryu, S. H. Ahn, J. Yang, *Smart Mater. Struct.* **2018**, *27*, 11LT01.

[55] C. Majidi, *Adv. Mater. Technol.* **2019**, *4*, 1800477.

[56] J. Lee, H. Kwon, J. Seo, S. Shin, J. H. Koo, C. Pang, S. Son, J. H. Kim, Y. H. Jang, D. E. Kim, T. Lee, *Adv. Mater.* **2015**, *27*, 2433.

[57] J. K. Lee, J. Ko, M. B. G. Jun, P. C. Lee, *Mater. Res. Express* **2016**, *3*, 025301.

[58] H. Asai, M. Kikuchi, N. Shimada, K. Nakane, *RSC Adv.* **2017**, *7*, 17593.

[59] N. Ogata, S. Yamaguchi, N. Shimada, G. Lu, T. Iwata, K. Nakane, T. Ogihara, *J. Appl. Polym. Sci.* **2007**, *104*, 1640.

[60] H. Z. Xu, T. Bronner, M. Yamamoto, H. Yamane, *Carbohydr. Polym.* **2018**, *201*, 182.

[61] A. Suzuki, K. Ohta, *J. Appl. Polym. Sci.* **2018**, 135.

[62] T. Fujii, Y. Mizutani, K. Nakane, *J. Appl. Polym. Sci.* **2018**, 135.

[63] H. Xu, B. Bauer, M. Yamamoto, H. Yamane, *Text. Res. J.* **2018**, *89*, 1770.

[64] M. de Ruijter, A. Ribeiro, I. Dokter, M. Castilho, J. Malda, *Adv. Healthcare Mater.* **2019**, *8*, 1800418.

[65] a) L. H. Zhang, X. P. Duan, X. Yan, M. Yu, X. Ning, Y. Zhao, Y. Z. Long, *RSC Adv.* **2016**, *6*, 53400; b) M. M. Bubakir, H. Li, A. Barhoum, W. Yang, in *Handbook of Nanofibers* (Eds: A. Barhoum, M. Bechelany, A. Makhlouf), Springer International Publishing, Cham, Switzerland **2018**, p. 1.

[66] X. Yan, X. P. Duan, S. X. Yu, Y. M. Li, X. Lv, J. T. Li, H. Y. Chen, X. Ning, Y. Z. Long, *RSC Adv.* **2017**, *7*, 33132.

[67] X. Yan, M. Yu, L.-H. Zhang, X.-S. Jia, J.-T. Li, X.-P. Duan, C.-C. Qin, R.-H. Dong, Y.-Z. Long, *Nanoscale* **2016**, *8*, 209.

[68] C.-C. Qin, X.-P. Duan, L. Wang, L.-H. Zhang, M. Yu, R.-H. Dong, X. Yan, H.-W. He, Y.-Z. Long, *Nanoscale* **2015**, *7*, 16611.

[69] M. L. Rivera, S. E. Hudson, in *Proc. 2019 CHI Conf. on Human Factors in Computing Systems*, (Eds: S. Brewster, G. Fitzpatrick), ACM, Glasgow, Scotland, UK **2019**, p. 1.

[70] J. Ko, V. Ahsani, S. X. Yao, N. K. Mohtaram, P. C. Lee, M. B. G. Jun, *J. Micromech. Microeng.* **2016**, *27*, 025007.

[71] N. Mayadeo, K. Morikawa, M. Naraghi, M. J. Green, *J. Polym. Sci., Part B: Polym. Phys.* **2017**, *55*, 1393.

[72] Z. Liu, H. Li, W. Wu, H. Chen, Y. Ding, W. Yang, *J. Polym. Eng.* **2015**, *35*, 61.

[73] C. J. Luo, S. D. Stoyanov, E. Stride, E. Pelan, M. Edirisinghe, *Chem. Soc. Rev.* **2012**, *41*, 4708.

[74] A. Doustgani, E. Ahmadi, *J. Ind. Text.* **2015**, *45*, 626.

[75] E. Zhmayev, D. Cho, Y. L. Joo, *Polymer* **2010**, *51*, 4140.

[76] Y. Qin, L. Cheng, Y. Zhang, X. Chen, X. Wang, X. He, W. Yang, Y. An, H. Li, *J. Appl. Polym. Sci.* **2018**, *135*, 46554.

[77] S.-X. Yu, J. Zheng, X. Yan, X.-X. Wang, G.-D. Nie, Y.-Q. Tan, J. Zhang, K.-Y. Sui, Y.-Z. Long, *Mater. Res. Express* **2018**, *5*, 045019.

[78] S. Zaiss, T. D. Brown, J. C. Reichert, A. Berner, *Materials* **2016**, *9*, 232.

[79] J. P. Murphy, M. C. Brockway, J. M. Andriolo, N. J. Sutton, J. L. Skinner, *MRS Commun.* **2018**, *8*, 1098.

[80] X. H. Li, W. M. Yang, H. Y. Li, Y. Wang, M. M. Bubakir, Y. M. Ding, Y. C. Zhang, *J. Appl. Polym. Sci.* **2015**, 132.

[81] R. Sidaraviciute, D. Buivydiene, E. Krugly, E. Valatka, D. Martuzevicius, *J. Photochem. Photobiol., A* **2019**, *368*, 7.

[82] T. F. Chala, C. M. Wu, M. H. Chou, Z. L. Guo, *ACS Appl. Mater. Interfaces* **2018**, *10*, 28955.

[83] B. Zhou, L. Li, L. J. Guo, L. L. Chen, B. Dong, C. H. Zhu, D. F. Hao, X. F. Hao, *J. Nanosci. Nanotechnol.* **2019**, *19*, 3012.

[84] Z. Li, Y. Yuan, B. Chen, Y. Liu, J. Nie, G. Ma, *J. Polym. Sci., Part A: Polym. Chem.* **2017**, *55*, 2815.

[85] Y. Xu, D. Wang, M. Zhang, H. Wang, Q. Wei, *Fibers Polym.* **2017**, *18*, 1981.

[86] T. Nazari, H. Garmabi, *J. Appl. Polym. Sci.* **2016**, 133.

[87] T. Nazari, H. Garmabi, *Polym. Int.* **2018**, *67*, 178.

[88] J. Ko, D. Kan, M. B. G. Jun, *Manuf. Lett.* **2015**, *3*, 5.

[89] A. Malakhov, A. Belousov, A. V. Bakirov, S. N. Chvalun, *Fibre Chem.* **2015**, *47*, 14.

[90] J. C. Singer, A. Ringk, R. Giesa, H.-W. Schmidt, *Macromol. Mater. Eng.* **2015**, *300*, 259.

[91] a) P. Xing, G. P. Robertson, M. D. Guiver, S. D. Mikhailenko, K. Wang, S. Kaliaguine, *J. Membr. Sci.* **2004**, *229*, 95; b) M. Gil, X. Ji, X. Li, H. Na, J. Eric Hampsey, Y. Lu, *J. Membr. Sci.* **2004**, *234*, 75.

[92] a) Z. Tahir, A. Ilyas, X. Li, M. R. Bilad, I. F. J. Vankelecom, A. L. Khan, *J. Appl. Polym. Sci.* **2018**, *135*, 45952; b) A. Iulianelli, C. Algieri, L. Donato, A. Garofalo, F. Galiano, G. Bagnato, A. Basile, A. Figoli, *Int. J. Hydrogen Energy* **2017**, *42*, 22138.

[93] R. I. Shekar, T. M. Kotresh, P. M. D. Rao, K. Kumar, *J. Appl. Polym. Sci.* **2009**, *112*, 2497.

[94] N. D. Govinna, T. Keller, C. Schick, P. Cebe, *Polymer* **2019**, *171*, 50.

[95] a) G. Hochleitner, F. Chen, C. Blum, P. D. Dalton, B. Amsden, J. Groll, *Acta Biomater.* **2018**, *72*, 110; b) F. Chen, G. Hochleitner, T. Woodfield, J. Groll, P. D. Dalton, B. G. Amsden, *Biomacromolecules* **2016**, *17*, 208.

[96] J. Fang, L. Zhang, D. Sutton, X. Wang, T. Lin, *J. Nanomater.* **2012**, *2012*, 1.

[97] J. N. Haigh, T. R. Dargaville, P. D. Dalton, *Mater. Sci. Eng., C* **2017**, *77*, 883.

[98] M. Bartnikowski, T. R. Dargaville, S. Ivanovski, D. W. Hutmacher, *Prog. Polym. Sci.* **2019**, *96*, 1.

[99] G. Hochleitner, M. Kessler, M. Schmitz, A. R. Boccaccini, J. Tessmar, J. Groll, *Mater. Lett.* **2017**, *205*, 257.

[100] a) K. S. Ramadan, D. Sameoto, S. Evoy, *Smart Mater. Struct.* **2014**, *23*, 033001; b) P. Martins, A. C. Lopes, S. Lanceros-Mendez, *Prog. Polym. Sci.* **2014**, *39*, 683.

[101] S. Florczak, T. Lorson, T. Zheng, M. Mrlik, D. W. Hutmacher, M. J. Higgins, R. Luxenhofer, P. D. Dalton, *Polym. Int.* **2019**, *68*, 735.

[102] B. Delalat, F. Harding, B. Gundsambuu, E. M. De-Juan-Pardo, F. M. Wunner, M.-L. Wille, M. Jasieniak, K. A. L. Malatesta, H. J. Griesser, A. Simula, D. W. Hutmacher, N. H. Voelcker, S. C. Barry, *Biomaterials* **2017**, *140*, 58.

[103] C. Paindelli, N. Navone, C. J. Logothetis, P. Friedl, E. Dondossola, *Biomaterials* **2019**, *197*, 296.

[104] A. Hammerl, C. E. Diaz Cano, E. M. De-Juan-Pardo, M. van Griensven, P. S. P. Poh, *Int. J. Mol. Sci.* **2019**, *20*, 1068.

[105] N. Abbasi, A. Abdal-hay, S. Hamlet, E. Graham, S. Ivanovski, *ACS Biomater. Sci. Eng.* **2019**, *5*, 3448.

[106] S. Bertlein, G. Hochleitner, M. Schmitz, J. Tessmar, M. Raghunath, P. D. Dalton, J. Groll, *Adv. Healthcare Mater.* **2019**, *8*, 1801544.

[107] J. N. Haigh, Y. M. Chuang, B. Farrugia, R. Hoogenboom, P. D. Dalton, T. R. Dargaville, *Macromol. Rapid Commun.* **2016**, *37*, 93.

[108] F. Kotz, P. Risch, K. Arnold, S. Sevim, J. Puigmartí-Luis, A. Quick, M. Thiel, A. Hrynevich, P. D. Dalton, D. Helmer, B. E. Rapp, *Nat. Commun.* **2019**, *10*, 1439.

[109] R. L. Mauck, B. M. Baker, N. L. Nerurkar, J. A. Burdick, W. J. Li, R. S. Tuan, D. M. Elliott, *Tissue Eng., Part B* **2009**, *15*, 171.

[110] X. Yu, J. Zhou, H. Liang, Z. Jiang, L. Wu, *Prog. Mater. Sci.* **2018**, *94*, 114.

[111] O. Bas, E. M. De-Juan-Pardo, M. P. Chhaya, F. M. Wunner, J. E. Jeon, T. J. Klein, D. W. Hutmacher, *Eur. Polym. J.* **2015**, *72*, 451.

[112] A. Van Mil, M. Castilho, M. Maher, C. H. Metz, R. G. C. Maas, G. Hochleitner, J. Groll, K. Ito, J. Malda, J. P. G. Sluijter, *Cardiovasc. Res.* **2018**, *114*, S112.

[113] O. Bas, E. M. De-Juan-Pardo, C. Meinert, D. D'Angella, J. G. Baldwin, L. J. Bray, R. M. Wellard, S. Kollmannsberger, E. Rank, C. Werner, T. J. Klein, I. Catelas, D. W. Hutmacher, *Biofabrication* **2017**, *9*, 025014.

1904664 (26 of 28)

**ADVANCED
SCIENCE NEWS**

www.advancedsciencenews.com

**ADVANCED
FUNCTIONAL
MATERIALS**

www.afm-journal.de

[114] a) J. G. Baldwin, F. Wagner, L. C. Martine, B. M. Holzapfel, C. Theodoropoulos, O. Bas, F. M. Savi, C. Werner, E. M. De-Juan-Pardo, D. W. Hutmacher, *Biomaterials* **2017**, *121*, 193; b) A. Abdal-Hay, N. Abbasi, M. Gwiazda, S. Hamlet, S. Ivanovski, *Eur. Polym. J.* **2018**, *105*, 257.

[115] M. J. Chen, L. S. Kimpton, J. P. Whiteley, M. Castilho, J. Malda, C. P. Please, S. L. Waters, H. M. Byrne, *Eur. J. Appl. Math.* https://doi.org/10.1017/S09567925180006571.

[116] M. Castilho, G. Hochleitner, W. Wilson, B. van Rietbergen, P. D. Dalton, J. Groll, J. Malda, K. Ito, *Sci. Rep.* **2018**, *8*, 1245.

[117] a) E. L. Gill, S. Willis, M. Gerigk, P. Cohen, D. Zhang, X. Li, Y. Y. S. Huang, *ACS Appl. Mater. Interfaces* **2019**, *11*, 19679; b) J. H. Jordahl, L. Solorio, H. Sun, S. Ramcharan, C. B. Teeple, H. R. Haley, K. J. Lee, T. W. Eyster, G. D. Luker, P. H. Krebsbach, J. Lahann, *Adv. Mater.* **2018**, *30*, 1707196.

[118] N. C. Paxton, J. Ren, M. J. Ainsworth, A. K. Solanki, J. R. Jones, M. C. Allenby, M. M. Stevens, M. A. Woodruff, *Macromol. Rapid Commun.* **40**, 1900019.

[119] K. Semjonov, A. Lust, K. Kogermann, I. Laidmae, S. L. Maunu, S. P. Hirvonen, J. Yliruusi, G. Nurk, E. Lust, J. Heinamaki, *Eur. J. Pharm. Sci.* **2018**, *121*, 260.

[120] Y. Huang, N. Bu, Y. Duan, Y. Pan, H. Liu, Z. Yin, Y. Xiong, *Nanoscale* **2013**, *5*, 12007.

[121] M. M. Bubakir, W. L. He, H. Y. Li, Y. M. Ding, W. M. Yang, *Key Eng. Mater.* **2017**, *717*, 104.

[122] L. Moroni, T. Boland, J. A. Burdick, C. De Maria, B. Derby, G. Forgacs, J. Groll, Q. Li, J. Malda, V. A. Mironov, C. Mota, M. Nakamura, W. Shu, S. Takeuchi, T. B. F. Woodfield, T. Xu, J. J. Yoo, G. Vozzi, *Trends Biotechnol.* **2018**, *36*, 384.

[123] L. C. Martine, B. M. Holzapfel, J. A. McGovern, F. Wagner, V. M. Quent, P. Hesami, F. M. Wunner, C. Vaquette, E. M. De-Juan-Pardo, T. D. Brown, B. Nowlan, D. J. Wu, C. O. Hutmacher, D. Moi, T. Oussenko, E. Piccinini, P. W. Zandstra, R. Mazzieri, J. P. Levesque, P. D. Dalton, A. V. Taubenberger, D. W. Hutmacher, *Nat. Protoc.* **2017**, *12*, 639.

[124] G. Tiwari, R. Tiwari, B. Sriwastawa, L. Bhati, S. Pandey, P. Pandey, S. Bannerjee, *Int. J. Pharm. Invest.* **2012**, *2*, 2.

[125] A. Santos, M. Sinn Aw, M. Bariana, T. Kumeria, Y. Wang, D. Losic, *J. Mater. Chem. B* **2014**, *2*, 6157.

[126] J. S. Chin, L. Madden, S. Y. Chew, D. L. Becker, *Adv. Drug Delivery Rev.* **2019**, https://doi.org/10.1016/j.addr.2019.03.006.

[127] F. L. He, X. D. Deng, Y. Q. Zhou, T. D. Zhang, Y. L. Liu, Y. J. Ye, D. C. Yin, *Polym. Adv. Technol.* **2019**, *30*, 425.

[128] K. Cao, Y. Liu, A. A. Olkhov, V. Siracusa, A. L. Iordanskii, *Drug Delivery Transl. Res.* **2018**, *8*, 291.

[129] Y. Liu, K. Cao, S. Karpova, A. Olkhov, A. Filatova, A. Zhulkina, A. Burkov, S. V. Fomin, D. S. Rosa, A. L. Iordanskii, *Macromol. Symp.* **2018**, *381*, 1800130.

[130] H. Lian, Z. Meng, *Bioact. Mater.* **2017**, *2*, 96.

[131] S. M. Davachi, B. S. Heidari, I. Hejazi, J. Seyfi, E. Oliaei, A. Farzaneh, H. Rashedi, *Carbohydr. Polym.* **2017**, *155*, 336.

[132] A. Rahman, P. W. Lee, X. T. Wang, C. Zhang, J. K. Pokorski, E. Baer, *Macromol. Mater. Eng.* **2017**, *302*, 1600304.

[133] Y. Xu, K. Li, Y. Liu, Y. An, C. Xing, *J. Appl. Polym. Sci.* **2019**, *136*, 47662.

[134] S. K. Bhullar, B. Kaya, M. B. G. Jun, *J. Polym. Environ.* **2015**, *23*, 416.

[135] B. L. Farrugia, T. D. Brown, Z. Upton, D. W. Hutmacher, P. D. Dalton, T. R. Dargaville, *Biofabrication* **2013**, *5*, 025001.

[136] E. B. Petcu, R. Midha, E. McColl, A. Popa-Wagner, T. V. Chirila, P. D. Dalton, *Biofabrication* **2018**, *10*, 032001.

[137] M. Castilho, A. van Mil, M. Maher, C. H. G. Metz, G. Hochleitner, J. Groll, P. A. Doevendans, K. Ito, J. P. G. Sluijter, J. Malda, *Adv. Funct. Mater.* **2018**, *28*, 1803151.

[138] M. Frega, M. Tedesco, P. Massobrio, M. Pesce, S. Martinoia, *Sci. Rep.* **2014**, *4*, 5489.

[139] N. Schaefer, D. Janzen, E. Bakirci, A. Hrynevich, P. D. Dalton, C. Villmann, *Adv. Healthcare Mater.* **2019**, *8*, 1801226.

[140] a) C. E. Holy, S. M. Dang, J. E. Davies, M. S. Shoichet, *Biomaterials* **1999**, *20*, 1177; b) M. E. Manwaring, J. F. Walsh, P. A. Tresco, *Biomaterials* **2004**, *25*, 3631; c) P. D. Dalton, J. Mey, *Front. Biosci.* **2009**, *14*, 769.

[141] F. Tourlomousis, C. Jia, T. Karydis, A. Mershin, H. Wang, D. M. Kalyon, R. C. Chang, *Microsyst. Nanoeng.* **2019**, *5*, 15.

[142] D. W. Hutmacher, T. B. F. Woodfield, P. D. Dalton, in *Tissue Engineering* (Eds: C. vanBlitterswijk, J. DeBoer), Elsevier, Amsterdam **2014**, Ch. 10, p. 311.

[143] A. Steier, A. Muñiz, D. Neale, J. Lahann, *Adv. Mater.* **31**, 1806898.

[144] B. M. Holzapfel, J. C. Reichert, J. T. Schantz, U. Gbureck, L. Rackwitz, U. Noth, F. Jakob, M. Rudert, J. Groll, D. W. Hutmacher, *Adv. Drug Delivery Rev.* **2013**, *65*, 581.

[145] J. E. Phillips, D. W. Hutmacher, R. E. Guldberg, A. J. Garcia, *Biomaterials* **2006**, *27*, 5535.

[146] S. Bertlein, D. Hikimoto, G. Hochleitner, J. Hümmer, T. Jungst, M. Matsusaki, M. Akashi, J. Groll, *Small* **2018**, *14*, 1701521.

[147] A. Fuchs, A. Youssef, A. Seher, G. Hochleitner, P. D. Dalton, S. Hartmann, R. C. Brands, U. D. A. Müller-Richter, C. Linz, *BMC Oral Health* **2019**, *19*, 28.

[148] A. Weigand, A. M. Boos, K. Tasbihi, J. P. Beier, P. D. Dalton, M. Schrauder, R. E. Horch, M. W. Beckmann, P. L. Strissel, R. Strick, *Breast Cancer Res.* **2016**, *18*, 32.

[149] N. K. Mohtaram, J. Ko, C. King, L. Sun, N. Muller, M. B.-G. Jun, S. M. Willerth, *J. Biomed. Mater. Res., Part A* **2015**, *103*, 2591.

[150] B. S. Kim, K. E. Park, M. H. Kim, H. K. You, J. Lee, W. H. Park, *Int. J. Nanomed.* **2015**, *10*, 485.

[151] P. T. Sudheesh Kumar, S. Hashimi, S. Saifzadeh, S. Ivanovski, C. Vaquette, *Mater. Sci. Eng., C* **2018**, *92*, 554.

[152] S. Liao, C. Theodoropoulos, K. A. Blackwood, M. A. Woodruff, S. D. Gregory, *Artif. Organs* **2018**, *42*, E43.

[153] a) M. W. Laschke, M. D. Menger, *Trends Biotechnol.* **2017**, *35*, 133; b) N. V. Mekhileri, K. S. Lim, G. C. J. Brown, I. Mutreja, B. S. Schon, G. J. Hooper, T. B. F. Woodfield, *Biofabrication* **2018**, *10*, 024103.

[154] M. L. Muerza-Cascante, A. Shokoohmand, K. Khosrotehrani, D. Haylock, P. D. Dalton, D. W. Hutmacher, D. Loessner, *Acta Biomater.* **2017**, *52*, 145.

[155] L. Muerza-Cascante, K. Khosrotehrani, D. Haylock, D. W. Hutmacher, D. Loessner, in *Comprehensive Biomaterials II*, Vol 5 (Ed: P. Ducheyne), Elsevier, Oxford, **2017**, Ch. 11, p. 187.

[156] S. Wu, H. Peng, X. Li, P. N. Streubel, Y. Liu, B. Duan, *Biofabrication* **2017**, *9*, 044106.

[157] D. Loessner, A. Rockstroh, A. Shokoohmand, B. M. Holzapfel, F. Wagner, J. Baldwin, M. Boxberg, B. Schmalfeldt, E. Lengyel, J. A. Clements, D. W. Hutmacher, *Biomaterials* **2019**, *190–191*, 63.

[158] B. A. Pereira, N. L. Lister, K. Hashimoto, L. Teng, M. Flandes-Iparraguirre, A. Eder, A. Sanchez-Herrero, B. Niranjan, M. Frydenberg, M. M. Papargiris, M. G. Lawrence, R. A. Taylor, D. W. Hutmacher, S. J. Ellem, G. P. Risbridger, E. M. De-Juan-Pardo, *Biomaterials* **2019**, *197*, 72.

[159] N. Bock, A. Shokoohmand, T. Kryza, J. Röhl, J. Meijer, P. A. Tran, C. C. Nelson, J. A. Clements, D. W. Hutmacher, *Bone Res.* **2019**, *7*, 13.

[160] T. Brückner, A. Fuchs, L. Wistlich, A. Hoess, B. Nies, U. Gbureck, *Materials* **2019**, *12*, 834.

[161] E. C. L. Bolle, N. Bartnikowski, P. Haridas, T. J. Parker, J. F. Fraser, S. D. Gregory, T. R. Dargaville, *J. Biomed. Mater. Res., Part B* **2019**, 1.

[162] A. Farag, S. M. Hashimi, C. Vaquette, F. Z. Volpato, D. W. Hutmacher, S. Ivanovski, *Arch. Oral Biol.* **2018**, *88*, 67.

[163] A. Farag, S. M. Hashimi, C. Vaquette, P. M. Bartold, D. W. Hutmacher, S. Ivanovski, *J. Clin. Periodontol.* **2018**, *45*, 586.

[164] E. Dondossola, S. Casarin, C. Paindelli, E. M. De-Juan-Pardo, D. W. Hutmacher, C. J. Logothetis, P. Friedl, *JNCI: J. Natl. Cancer Inst.* **2019**, https://doi.org/10.1093/jnci/djz007.

[165] a) L. Thibaudeau, V. M. Quent, B. M. Holzapfel, A. V. Taubenberger, M. Straub, D. W. Hutmacher, *Cancer Metastasis Rev.* **2014**, *33*, 721; b) L. Thibaudeau, A. V. Taubenberger, B. M. Holzapfel, V. M. Quent, T. Fuehrmann, P. Hesami, T. D. Brown, P. D. Dalton, C. A. Power, B. G. Hollier, D. W. Hutmacher, *Dis. Models Mech.* **2014**, *7*, 299.

[166] N. P. Holzapfel, A. Shokoohmand, F. Wagner, M. Landgraf, S. Champ, B. M. Holzapfel, J. A. Clements, D. W. Hutmacher, D. Loessner, *Am. J. Cancer Res.* **2017**, *7*, 1322.

[167] M. Landgraf, J. A. McGovern, P. Friedl, D. W. Hutmacher, *Trends Biotechnol.* **2018**, *36*, 242.

[168] E. Dondossola, S. Alexander, B. M. Holzapfel, S. Filippini, M. W. Starbuck, R. M. Hoffman, N. Navone, E. M. De-Juan-Pardo, C. J. Logothetis, D. W. Hutmacher, P. Friedl, *Sci. Transl. Med.* **2018**, *10*, eaao5726.

[169] F. Wagner, B. M. Holzapfel, J. A. McGovern, A. Shafiee, J. G. Baldwin, L. C. Martine, C. A. Lahr, F. M. Wunner, T. Friis, O. Bas, M. Boxberg, P. M. Prodinger, A. Shokoohmand, D. Moi, R. Mazzieri, D. Loessner, D. W. Hutmacher, *Biomaterials* **2018**, *171*, 230.

[170] L. Thibaudeau, A. Taubenberger, B. M. Holzapfel, V. M. Quent, T. Fuehrmann, P. Hesami, T. D. Brown, P. D. Dalton, C. A. Power, B. Hollier, D. W. Hutmacher, *Dis. Models Mech.* **2014**, *7*, 299.

[171] A. Shafiee, J. A. McGovern, C. A. Lahr, C. Meinert, D. Moi, F. Wagner, M. Landgraf, E. De-Juan-Pardo, R. Mazzieri, D. W. Hutmacher, *Int. J. Cancer* **2018**, *143*, 1470.

[172] J. A. McGovern, M. Griffin, D. W. Hutmacher, *Dis. Models Mech.* **2018**, *11*, dmm033084.

[173] E. Dondossola, B. M. Holzapfel, S. Alexander, S. Filippini, D. W. Hutmacher, P. Friedl, *Nat. Biomed. Eng.* **2016**, *1*, 0007.

[174] M. R. Beaulieu, N. R. Hendricks, J. J. Watkins, *ACS Photonics* **2014**, *1*, 799.

[175] J. Ko, S. Bhullar, Y. Y. Cho, P. C. Lee, M. B. G. Jun, *Smart Mater. Struct.* **2015**, *24*, 075027.

[176] Q. Chen, X. Mei, Z. Shen, D. Wu, Y. Zhao, L. Wang, X. Chen, G. He, Z. Yu, K. Fang, D. Sun, *Opt. Lett.* **2017**, *42*, 5106.

[177] X. Yu, M. Feng, R. Zhang, Y. Feng, H. You, F. Guo, S. Chen, D. Zhang, *Org. Electron.* **2017**, *51*, 442.

[178] V. Sans, V. Dragone, L. Cronin, in *Green Chemical Engineering*, Vol. *12* (Ed: A. Lapkin), Wiley-VCH, Weinheim **2018**, Ch. 9, p. 218.

[179] J. P. Murphy, B. M. Ross, J. M. Andriolo, J. L. Skinner, *J. Vac. Sci. Technol. B* **2016**, *34*, 06KM01.

[180] A. Kojima, K. Teshima, Y. Shirai, T. Miyasaka, *J. Am. Chem. Soc.* **2009**, *131*, 6050.

[181] K. A. Bush, A. F. Palmstrom, Z. J. Yu, M. Boccard, R. Cheacharoen, J. P. Mailoa, D. P. McMeekin, R. L. Z. Hoye, C. D. Bailie, T. Leijtens, I. M. Peters, M. C. Minichetti, N. Rolston, R. Prasanna, S. Sofia, D. Harwood, W. Ma, F. Moghadam, H. J. Snaith, T. Buonassisi, Z. C. Holman, S. F. Bent, M. D. McGehee, *Nat. Energy* **2017**, *2*, 17009.

[182] Y. Shen, S. A. Xia, P. F. Yao, R. H. Gong, Q. S. Liu, B. Y. Deng, *Fibers Polym.* **2017**, *18*, 1568.

[183] Y. An, S. Yu, S. Li, X. Wang, W. Yang, M. Yousefzadeh, M. M. Bubakir, H. Li, *Fibers Polym.* **2018**, *19*, 2507.

[184] Z.-Z. Fan, H.-W. He, X. Yan, R.-H. Zhao, Y.-Z. Long, X. Ning, *Polymers* **2019**, *11*, 530.

[185] G. Xie, Z. Chen, S. Ramakrishna, Y. Liu, *J. Appl. Polym. Sci.* **2015**, *132*, 42574.

[186] B. K. Gale, A. R. Jafek, C. J. Lambert, B. L. Goenner, H. Moghimifam, U. C. Nze, S. K. Kamarapu, *Inventions* **2018**, *3*, 60.

[187] K. S. Lim, M. Baptista, S. Moon, T. B. F. Woodfield, J. Rnjak-Kovacina, *Trends Biotechnol.*, https://doi.org/10.1016/j.tibtech.2019.04.004.

[188] B. Grigoryan, S. J. Paulsen, D. C. Corbett, D. W. Sazer, C. L. Fortin, A. J. Zaita, P. T. Greenfield, N. J. Calafat, J. P. Gounley, A. H. Ta, F. Johansson, A. Randles, J. E. Rosenkrantz, J. D. Louis-Rosenberg, P. A. Galie, K. R. Stevens, J. S. Miller, *Science* **2019**, *364*, 458.

[189] J. Zeng, H. Wang, Y. Lin, J. Zhang, F. Liang, F. Fang, F. Yang, P. Wang, Z. Zhu, X. Chen, X. Chen, Z. Wang, N. Cai, Y. Tang, P. Wu, *Microfluid. Nanofluid.* **2018**, *22*, 23.

[190] a) D. Lv, M. M. Zhu, Z. C. Jiang, S. H. Jiang, Q. L. Zhang, R. H. Xiong, C. B. Huang, *Macromol. Mater. Eng.* **2018**, *303*, 1800336; b) B. Zhang, J. K. He, X. Li, F. Y. Xu, D. C. Li, *Nanoscale* **2016**, *8*, 15376; c) D. Ye, Y. J. Ding, Y. Q. Duan, J. T. Su, Z. P. Yin, Y. A. Huang, *Small* **2018**, *14*, 1703521; d) R. Tan, X. Yang, Y. Shen, *Rob. Biomimetics* **2017**, *4*, 17.